FULLY SOFTENED SHEAR STRENGTH MEASUREMENT AND EMPIRICAL CORRELATIONS

Timothy D. Stark, Ph.D., P.E., D. GE, F. ASCE
Professor of Civil and Environmental Engineering
University of Illinois at Urbana-Champaign
205 N. Mathews Ave.
Urbana, IL 61801
(217) 333-7394
(217) 333-9464 Fax
Email: tstark@illinois.edu

and

Rodrigo Fernandez, S.M. ASCE
Graduate Research Assistant of Civil and Environmental Engineering
University of Illinois at Urbana-Champaign
205 N. Mathews Ave.
Urbana, IL 61801
Email: frnndzs2@illinois.edu

A technical paper **SUBMITTED** for review and possible publication in the ASCE *Journal of Geotechnical and Geoenvironmental Engineering*

April 24, 2018

FULLY SOFTENED SHEAR STRENGTH MEASUREMENT AND EMPIRICAL CORRELATION

Timothy D. Stark[1] and Rodrigo Fernandez[2]

ABSTRACT: Laboratory measured fully softened strength (FSS) is used to represent the mobilized drained strength in first-time slope failures in overconsolidated, compacted, and desiccated fine-grained soils. The FSS is used to represent the mobilized drained strength remaining after the effects of mechanical overconsolidation, compaction, desiccation, and/or other strengthening processes have been significantly reduced or removed due to applied shear stresses, wet-dry cycles, swelling, freeze-thaw cycles, stress relief, and/or weathering. This paper shows that drained laboratory ring shear and direct shear tests yield similar values of FSS, which are lower than FSSs measured using consolidated-drained triaxial compression tests. A conversion factor is presented to convert ring shear and direct shear derived FSSs to the triaxial compression mode of shear to simulate the field mode of shear and mobilized FSS in "first time" slope failures. This paper also compares various FSS empirical correlations and presents recommendations for using FSS correlations for design of embankments, dams, levees, and natural and cut slopes.

Keywords: Fully softened shear strength, index properties, empirical correlations, effective normal stress, power function, direct shear, slope stability

[1] Professor, Dept. of Civil and Environmental Engineering, Univ. of Illinois, 205 N. Mathews Ave., Urbana, IL 61801-2352. E-mail: tstark@illinois.edu

[2] Graduate Research Assistant, Dept. of Civil and Environmental Engineering, Univ. of Illinois, 205 N. Mathews Ave., Urbana, IL 61801-2352. E-mail: frnndzs2@illinois.edu

INTRODUCTION

Skempton (1970; 1977) uses a regressive analysis of various first-time slope failures involving cut slopes in brown London Clay to show that the mobilized drained strength is less than the drained peak strength but greater than the drained residual strength for a pore-water pressure ratio (r_u) ranging from 0.15 to 0.35 with an average of 0.3 (see **Figure 1**). To develop a design procedure, Skempton (1977) had to relate this mobilized drained strength to a drained strength that could be easily and consistently measured in a commercial laboratory. To achieve this objective, Skempton (1977) observed that this mobilized drained strength is in reasonable agreement with the drained peak shear strength measured using a reconstituted and normally consolidated specimen of the fine-grained soil, i.e., fully softened strength (FSS), involved in the first-time slide.

Skempton (1970) tries to corroborate the use of the peak strength of a reconstituted and normally consolidated specimen for design by relating it to the critical state strength described by Schofield and Wroth (1968), which is the drained strength at unlimited shearing and constant volume. This analogy is made because Schofield and Wroth (1968) report that the peak strength of a reconstituted and normally consolidated London Clay specimen occurs before the critical state is reached, i.e., conservative, and can be measured in the laboratory. They also suggest that the value of critical state friction angle (ϕ'_c) for brown London Clay is 22.5^0. Skempton (1970) states that the laboratory FSS friction angle (ϕ'_{FSS}) of brown London Clay is 20^0, i.e., the peak strength of a normally consolidated specimen. Skempton (1970) concludes that ϕ'_{FSS} is a practical approximation of the mobilized drained friction angle (ϕ'_{mob}) of 21^0 and ϕ'_c. of 22.5^0.

In particular, **Figure 1** presents a comparison of the mobilized drained strength values for the various case histories involving brown London Clay reported by Skempton (1977) and drained strengths from various laboratory shear tests. **Figure 1** shows the drained peak strength measured using 38 mm diameter triaxial compression and 60 mm square direct shear specimens is too high (c'_{peak} = 14 kPa and $\phi'_{peak} = 20^0$) because the test specimens do not include a representative assemblage of joints and fissures (Skempton, 1977). The drained peak strength measured using 250 mm diameter triaxial compression specimens is lower (c'_{peak} = 7 kPa and $\phi'_{peak} = 20^0$) but still exceeds the mobilized drained strength (c'_{mob} = 0 kPa and $\phi'_{mob} = 21^0$) from the various brown London Clay case histories using the best fit line shown in **Figure 1**.

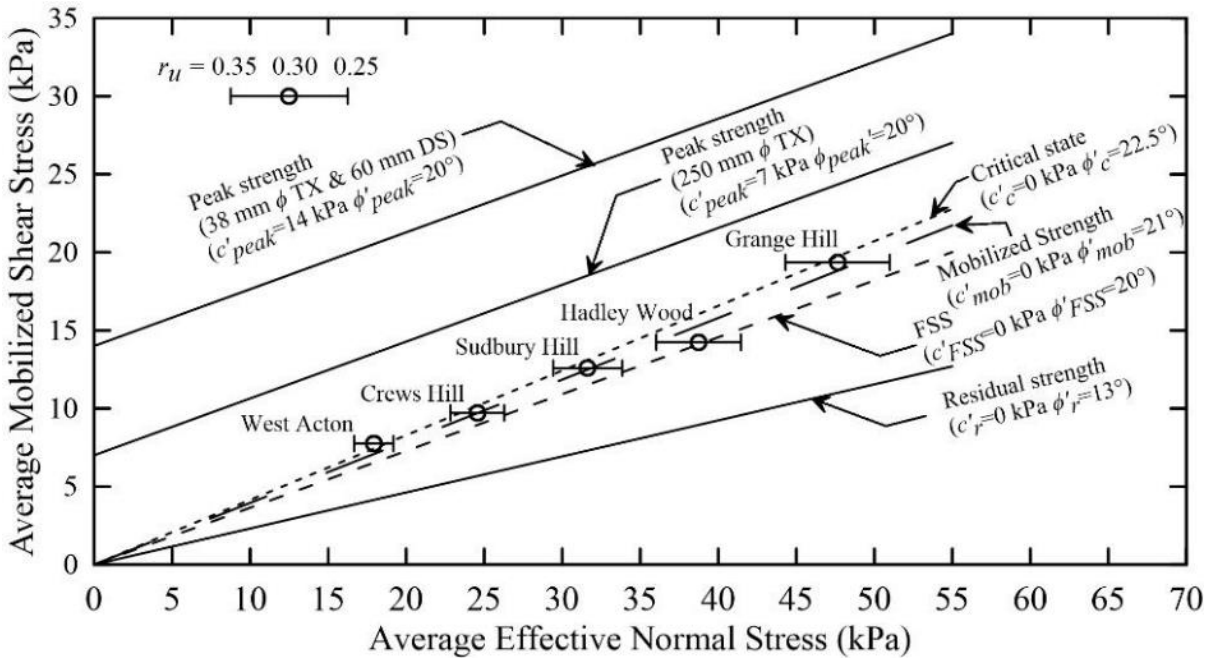

Figure 1: Mobilized drained shear strength in first-time slope failures in brown London Clay and comparison with the results of drained laboratory shear tests.

The peak shear strength of a reconstituted and normally consolidated specimen primarily from consolidated-drained (CD) and consolidated-undrained (CU) triaxial compression (TX) tests with pore-water pressure measurements (Bishop et al., 1965), corresponds to strength parameters (c'_{FSS} = 0 kPa and $\phi'_{FSS} = 20^0$), which is slightly lower than the mobilized strength parameters (c'_{mob} = 0 kPa and $\phi'_{mob} \sim 21^0$). Skempton (1977) reasoned that the slightly lower laboratory measured strength, i.e., ϕ'_{FSS}, and the highest foreseeable r_u provides a suitable/conservative design against long-term first-time failures in stiff, fissured clays.

The FSS also has been used to explain failures in desiccated and compacted soil slopes (Stark and Duncan, 1991; Stark and Eid, 1997; Duncan et al., 2011) subjected to applied shear stresses, repeated cycles of water intrusion and posterior dilation that can lead to formation of shrinkage cracks, water infiltration, swelling, and softening (Terzaghi, 1936; Kayyal and Wright, 1991; Wright, 2005; Wright et al., 2007). Infiltrating water can cause the soil to swell under zero pressure along the walls of open shrinkage cracks and lead to the outer portions of the slope becoming saturated and trapping air in the deeper portions of the slope (Terzaghi, 1936 and Terzaghi et al., 1996). The trapped air creates soil suction, which can lead to additional water being absorbed and further soil softening (Terzaghi et al., 1996). This nonuniform swelling weakens the soil, which allows new cracks, infiltration, progressive softening, and strength loss (Terzaghi, 1936).

(a) ***Critical State Strength***

The values of ϕ'_{FSS} and ϕ'_{c} from **Figure 1** are summarized in **Table 1** to facilitate describing the FSS. In theory, the value of ϕ'_{FSS} should be greater than ϕ'_{c} because it is measured at a smaller

shear displacement than ϕ'_c, which occurs at unlimited shearing and constant volume. However, **Table 1** shows that ϕ'_c for brown London Clay is 1.5^0 higher than ϕ'_{mob}. This is probably due to unlimited shearing and constant volume not occurring in the field during the drained case histories studied by Skempton (1970). Therefore, the use of ϕ'_c for brown London Clay could be unconservative for a given pore-water pressure ratio, which agrees with Skempton (1970) recommending use of ϕ'_{FSS}.

Table 1. Comparison of brown London Clay shear strength parameters.

Drained Shear Strength	**Effective Stress Cohesion (kPa)**	**Effective Stress Cohesion (degrees)**	**Reference**
Peak using 38 mm diameter specimen ($\phi'_{peak,small}$)	14	20	Bishop et al. (1965)
Peak using 250 mm diameter specimen ($\phi'_{peak,large}$)	7	20	Bishop et al. (1965)
Critical State (ϕ'_c)	0	22.5	Schofield and Wroth (1968)
Mobilized strength (ϕ'_{mob})	0	21	Skempton (1977)
Laboratory FSS (ϕ'_{FSS})	0	20	Skempton (1970)
Residual (ϕ'_r)	0	13	Skempton (1977)

The important comparison in **Table 1** is the only one (1) degree difference between ϕ'_{mob} and ϕ'_{FSS}, which reinforces Skempton's (1977) recommendation of using ϕ'_{FSS} to represent ϕ'_{mob} because it is slightly conservative, i.e., lower than ϕ'_{mob}, and can be readily measured in the laboratory. The authors also believe that the use of ϕ'_{FSS} is more logical because the drained field case histories do not appear to have undergone unlimited shearing at constant volume, i.e., achieved a critical state, so ϕ'_c is not applicable and it is greater than ϕ'_{mob}. **Table 1** also shows there is a 2.5^o difference between ϕ'_c and ϕ'_{FSS}. This is probably due to the difference in strength

criteria, testing condition, shearing under constant volume, and specimen stress history used to measure ϕ'_c. More importantly, this 2.5° difference between ϕ'_c and ϕ'_{FSS} is different than the 2.5° difference discussed below between the FSS measured using triaxial compression and ring shear modes of shear.

(b) ***Other FSS Confirmations***

Cooper et al. (1998) use the results of an induced first-time failure of a cut slope in stiff Gault clay to show that Skempton's (1977) empirical approach and laboratory measured ϕ'_{FSS} yields a reasonable design method. Conversely, Crabb and Atkinson (1991) show that the mobilized drained strength for first time slides with depths less than 2 m is in agreement with ϕ'_c and not ϕ'_{FSS}. Subsequently, Take and Bolton (2011) use centrifuge tests to show that seasonal wetting and drying, and the associated incremental ratcheting creep, dilation, and softening, beneath model slopes mobilized a drained strength less than the peak value but greater than ϕ'_c. Some of this variability in the drained mobilized strength may be due to uncertainties in the pore-water pressure conditions and/or centrifuge testing conditions, such as, scale effects, sample preparation, and test differences, that attempt to simulate the field conditions in Skempton's (1977) inverse analyses. In fact, Stark and Eid (1997) and Mesri and Shahien (2003) show that the mobilized strength in first time slides can be lower than the FSS at least along portions of the failure surface due to progressive failure. Therefore, Skempton's (1977) suggestion of using ϕ'_{mob} or ϕ'_{FSS} for the depth of soil that is subjected to the environmental and shear conditions that result in a FSS and the highest foreseeable r_u still provides a suitable/conservative design against long-term first-time failures in stiff, fissured clays.

FSS MODE OF SHEAR

Stark and Eid (1997) conclude that the relevant mode of shear for failure surfaces in first-time slides in natural cut slopes and compacted embankments is closer to drained triaxial compression (ASTM D7181) than torsional ring shear (RS) using ASTM D7608 or direct shear (DS) using ASTM D3080 because there is no well-defined failure surface and the random nature of the particle structure of a fully softened fine-grained soil. Using the results of Consolidated-Drained (CD) triaxial compression tests on five different fine-grained soils (see **Table 2**) at effective confining pressures of 70 and 275 kPa, Eid (1996) introduced an increase of 2.5° to convert the ring shear FSS secant friction angles to CD triaxial compression (CD-TX) FSS secant friction angles. Therefore, the RS fully softened secant friction angles (ϕ'_{FSS}) presented in subsequent FSS correlations (Stark et al. 2005; Stark and Hussain 2013; Gamez and Stark, 2014) were increased by 2.5° to reflect a CD-TX mode of shear (see **Figure 2**). This FSS correlation relates liquid limit (LL) measured using ASTM D4318 and clay-size fraction (CF) using % < 0.002 mm (ASTM D7928) to FSS secant friction angle as a function of effective normal stress for sixty (60) soils (see table in **Appendix A**, which highlights the thirteen (13) new soils tested since Gamez and Stark (2014) with a "^" symbol.

Table 2. Difference in secant FSS friction angles from RS and CD triaxial compression (from Eid, 1996).

Soil Name	Liquid Limit	Clay-Size Fraction (%<0.002 mm)	FSS Friction Angle Difference (degrees) at 70 kPa	FSS Friction Angle Difference (degrees) at 275 kPa
Urbana Till	24	18	2.6º	2.8º
Panoche Shale*	**53**	**50**	**1.9º**	**1.6º**
Pepper Shale	94	77	2.1º	3.3º
Oahe Shale #1	138	78	3.0º	2.7º

Oahe Shale #2*	**192**	**65**	**2.9º**	**1.7º**

NOTE: *Largest Deviation from the 2.5° conversion proposed by Stark and Eid (1997)

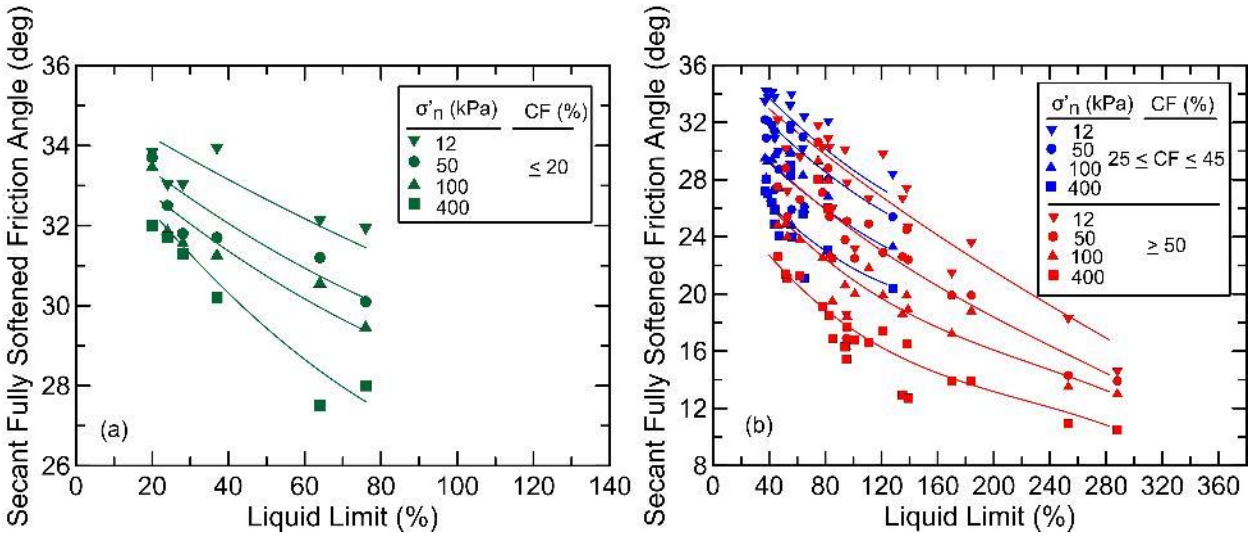

Figure 2: Updated drained fully softened secant friction angle correlation for: (a) CF ≤ 20% and (b) CF > 20%.

(a) Empirical FSS Correlation

The four trend lines in each CF group in **Figure 2** can be used to create a FSS strength envelope for use in stability analyses that represents the CD-TX mode of shear to analyze non-circular or compound failure surfaces. The FSS strength envelope is constructed using the estimated FSS secant friction angle, effective normal stresses of 0, 12, 50, 100, and 400 kPa, and calculating the corresponding FSS shear stress. For stability analyses, the entire strength envelope should be used to estimate the applicable shear strengths along the shallow non-circular failure surfaces as discussed in detail below.

Figure 2 shows three CF groups are used to distinguish the boundaries between rolling shear (≤ 20%), transitional shear (25% ≤ CF ≤ 45%), and sliding shear (≥ 50%) behavior, respectively. These three CF groupings are similar to those used by Lupini et al. (1981) and Skempton (1985), which are: CF ≤ 25%, 25% ≤ CF ≤ 50%, CF ≥ 50%, to delineate rolling, transitional, and sliding shear behavior, respectively. The available FSS data generated in this ongoing research does not demonstrate a distinct boundary between rolling and transitional shear and thus there is a gap in the clay-size groupings between less than or equal to 20% and greater than or equal to 25% as shown in **Figure 2**. A distinct or rigid transition from transitional to sliding shear behavior also was not observed and thus there is a small gap in the CF groupings between greater than or equal to 45% and greater than 50%. Interpolation can be used to estimate the FSS secant friction angle between the three CF groups in **Figure 2** for a particular effective normal stress.

In this FSS correlation, the liquid limit is used as an indicator of clay mineralogy and thus particle size. As the particle size decreases, the particle surface area and LL increase, and the drained FSS decreases. However, CF remains an important FSS predictive parameter because it indicates the quantity of the clay mineralogy and thus the type of shear behavior, i.e., rolling shear, transitional shear, and sliding shear, that is expected to occur.

(b) CD-TX mode of shear conversion factor

The difference between RS and CD-TX secant friction angles ranges from 1.6° to 3.3° (see **Table 2**), so Stark and Eid (1997) selected an average conversion factor of 2.5°. This conversion of 2.5° to a CD-TX mode of shear reflects some of the differences in the TX and RS test conditions

including: soil anisotropy, different consolidation conditions, laboratory testing boundary conditions, and failure surfaces that may not exist in the field as discussed in the next section.

Figure 3 shows values of FSS measured using RS and CD-TX tests as a function of effective normal stress for the five soils tested by Eid (1996) and twenty-five (25) additional soils. A best-fit line through the data is shown in red, which corresponds to the average difference in FSS friction angle for each effective normal stress. Each average value has an associated error bar, which corresponds to two (2) standard errors (standard deviation divided by the square root of the number of data points) of the mean of the data.

Figure 3 also includes a dashed line that corresponds to the RS and CD-TX friction angle difference of 2.5°. This trend line shows the average mode of shear conversion factor varies from 3.0° at effective normal stress of 50 kPa to about 2.0° at 400 kPa, depending on the CF. This 0.5° difference from the original 2.5° at high effective normal stresses is not significant because the tangent of 0.5° is small (0.009) and first-time slope failures in compacted soils and some natural slopes are shallow and do not involve high effective normal stress.

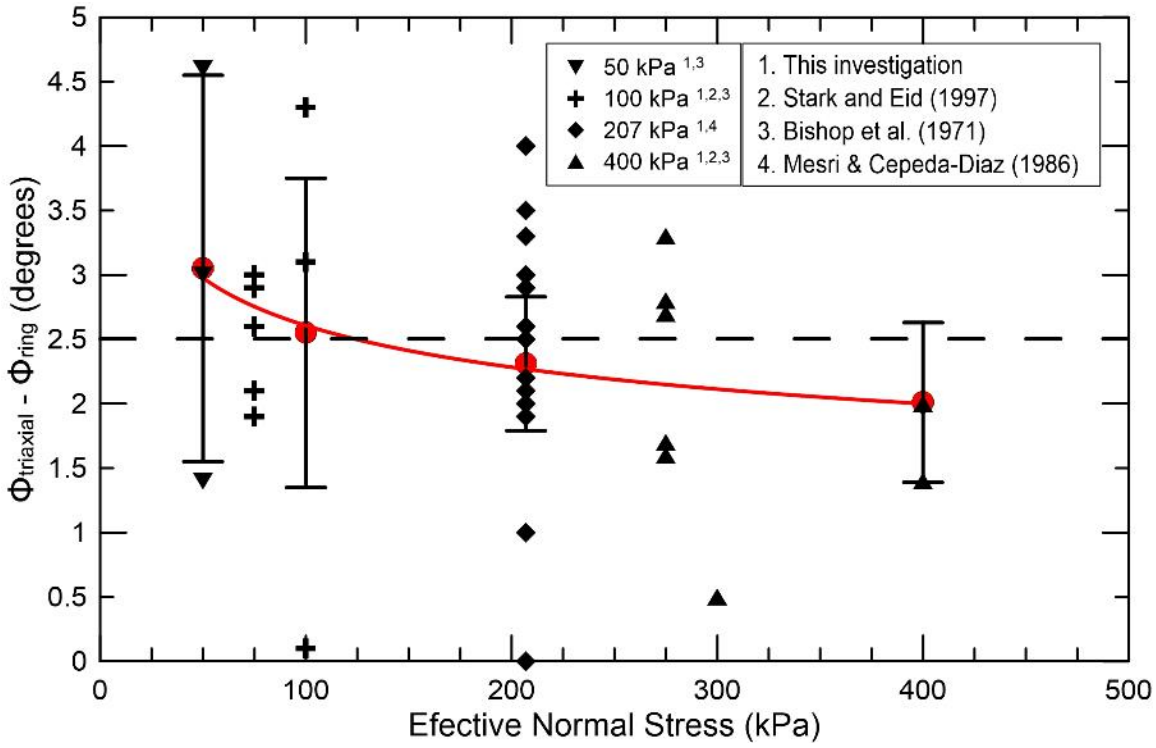

Figure 3: Comparison of fully softened secant angles obtained from CD triaxial compression and RS tests.

At low effective normal stresses this 0.5° difference from the original 2.5° is also not significant because the effective normal stresses on shallow failure surfaces are usually below 100 kPa due to high values of r_u generated primarily by precipitation so the tangent of the tangent of 0.5° is multiplied by a low effective normal stresses acting on the shallow failure surface. Therefore, the FSS at low effective normal stresses is more important for first time slides, which prompted extension of the FSS correlation in **Figure 2** to an effective normal stress of 12 kPa by Gamez and Stark (2014). Eid and Rabie (2017) also propose a FSS correlation using the 2.5° correction for the CD-TX mode of shear and a correlation extending to 10 kPa.

In summary, a 0.5° difference in the FSS conversion factor at effective normal stresses greater than and less than 100 kPa does not have a significant impact on calculated values of FS for observed shallow first-time failure surfaces. Therefore, the average conversion factor of 2.5° proposed by Eid (1996) is still reasonable for converting the RS and DS mode of shear to the CD-TX mode of shear. However, practitioners can use the correlation and adjust the estimated values of FSS secant friction angle for a different conversion factor than the original 2.5° using the relevant effective normal stress and the data in **Figure 3**.

Figure 4 shows the strength envelopes from FSS testing on Panoche Shale from Eid (1996). The strength envelope from CD-TX tests is approximately 2.0° higher than the DS and RS strength envelopes, which also confirms the average conversion factor of 2.5°. **Figure 4** also shows the strength envelopes measured using RS and DS are in close agreement, which is expected because of the similar horizontal shearing as discussed in detail below.

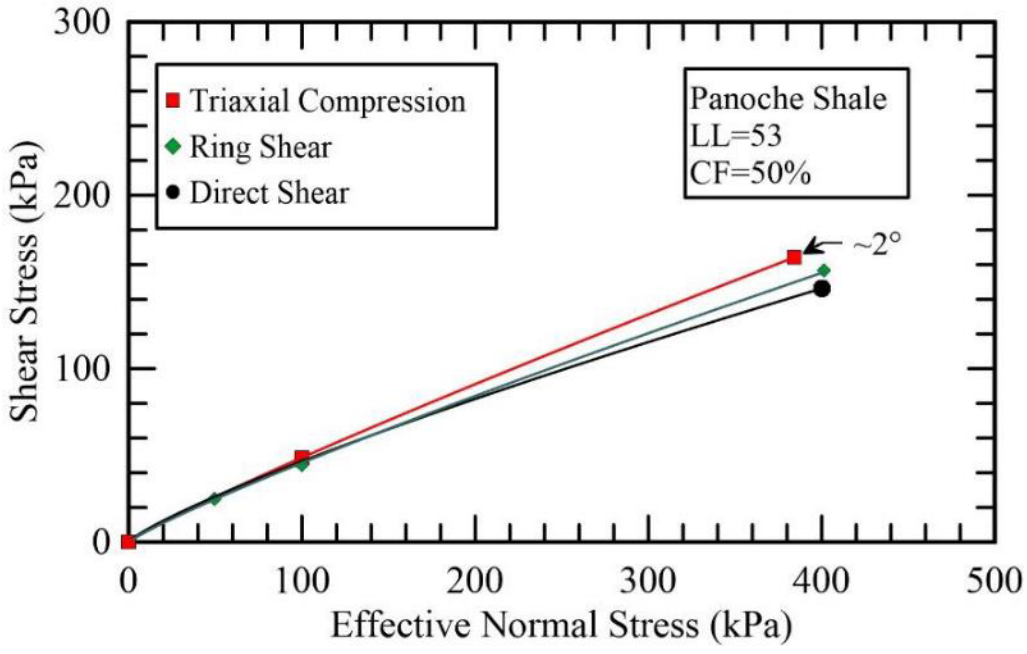

Figure 4: FSS strength envelopes for Panoche Shale from CD triaxial, ring shear, and direct shear FSS tests.

Figure 1 shows the difference between the drained mobilized strength from case histories (c'_{mob} = 0 kPa and $\phi'_{mob} \sim 21^0$) and the FSS measured using CD and CU triaxial compression (TX) tests (c'_{FSS} = 0 kPa and $\phi'_{FSS} = 20^0$) primarily from Bishop et al. (1965) is about one (1) degree. This one (1) degree difference reinforces that TX tests yield strengths that are in agreement with the mobilized drained strength and is the mode of shear primarily involved in first-time slope failures. Therefore, if a designer does not increase the value of FSS measured using a RS device it would be conservative by about 3.5^0 (1^0 plus 2.5^0) lower than the mobilized friction angle shown in **Figure 1**. The laboratory measured values of FSS should be lower than the drained mobilized strength because portions of the failure surface may not be at the laboratory FSS because weathering and applied shear stresses may not have completely softened the soil to a reconstituted and normally consolidation condition. In other words, all of the soil along the failure surface may not be representative of a reconstituted and normally consolidated material because the weathering and softening is not uniform and has not been completed.

MEASUREMENT OF LABORATORY FSS

The FSS has been measured using the CD TX test (Gibson 1953; Bishop et al. 1965; Skempton 1977). However, a number of challenges exist with performing CD TX tests (ASTM D7181) on a normally consolidated specimen, especially at low confining pressures to simulate a shallow failure surface. These challenges include supporting the weak specimen during test set-up and before application of the cell pressure, the time to and difficulty in back-pressure saturating the fine-grained specimen, and applying drained shear because of the low hydraulic conductivity of

the fine grained soil. Because of the time required for back-pressure saturation (Skempton, 1954) and drained shearing in CD TX tests, CU-TX tests are frequently used in practice. However, values of FSS measured using CU-TX tests are frequently higher (at least five degrees) than CD-TX tests probably due to a lack of saturation and thus a higher effective stress during shearing (see Figure 5.44 in Duncan et al., 2014). As a result, values of FSS from CU-TX tests with pore-water pressure measurements tend to be unconservative and should be verified or reduced using the empirical correlation in **Figure 2** before use in practice.

Due to difficulties with CD-TX and CU-TX testing, the RS and DS devices have been used to measure the FSS even though they fail the specimen along a nearly horizontal surface, which does not simulate field conditions in first-time slides. Because both tests apply the same mode of shear to the specimen (horizontal shear), it was anticipated that both devices would yield similar values of FSS (Eid, 1996).

However, RS and DS tests should yield different values of FSS than CD-TX because of differences in consolidation conditions, soil particle structure, mode of shear, soil anisotropy, boundary conditions, soil extrusion, friction during shear, and degree of saturation prior to shear. For example, a CD-TX specimen is isotropically consolidated whereas as RS and DS specimens are anisotropically consolidated due to being consolidated in a rigid specimen container. This results in more edge to face particle arrangement in the horizontal direction in the RS and DS tests than CD-TX tests because of the lower lateral pressure, which usually results in lower values of FSS. The CD-TX specimen is back-pressure saturated prior to shearing whereas the RS and DS specimen is mixed into a paste and normally consolidated, which can result in a partially saturated

specimen, especially if the specimen is not prepared at or near the liquid limit and is tested at a low effective normal stress. In fact, Duncan et al. (2014) state on page 74 that:

> "It is clear that the triaxial tests produced higher friction angles than the direct shear test.".

However, sometimes the RS and DS devices yield values of FSS that are similar to or higher than CD-TX values, which is probably due to the RS and DS specimens not being saturated or errors during testing errors as discussed below.

(a) Comparison of RS and DS FSS Testing

Eid (1996) investigated the values of FSS measured using these two horizontal shear surface devices by performing DS and RS tests on Panoche Shale and Lower Pepper Shale over twenty years ago. **Figure 5** presents the shear stress ratio (shear stress divided by effective normal stress)-shear displacement relationships for Panoche Shale from Eid (1996), which shows the difference in measured stress ratio between RS and DS devices is less than 0.5°.

Additional FSS testing was performed herein in to compare RS and DS test results and reinforces that RS and DS tests yield similar values that are less than CD-TX. This testing also confirmed that RS tests are completed significantly faster and easier than DS tests because the DS specimen requires a much longer consolidation time and slower shear displacement rate due to the longer drainage path from the middle of the specimen than in the RS device, where failure occurs just

below the upper porous disc. This RS and DS comparison also resulted in observing the following challenges and possible errors with using a DS device to measure the FSS:

- Consolidation of a normally consolidated specimen can result in insufficient material remaining in the upper shear box before shearing is started due to specimen consolidation,
- Tilting of the top platen or upper shear box, which causes friction and additional resistance as discussed in detail below,
- A gap developing on the leading edge of the DS specimen during shear due to the deformation required to mobilize the passive resistance of a normally consolidated soil,
- Maintaining a gap between the upper and lower shear boxes because of the normally consolidated nature of the specimen,
- Progressive failure of the DS specimen due to the normally consolidated specimen undergoing variable deformations during shear,
- Variable cross-sectional area during shear,
- Soil extrusion through the gap,
- The top shear box not being fixed to the top platen (see Stark, 2017).

Tilting of the top shear box during shear can lead to friction developing between the upper and lower shear boxes, which leads to overestimation of the FSS. The tilting of the top platen and/or upper shear box is caused by, among other things, opening a gap between the upper and lower shear boxes and the unconsolidated specimen deforming due the applied normal stress, differential consolidation, soil extrusion during shear, non-uniform soil swelling before and during shear, and mis-alignment of the shear boxes before and during shear. The friction between the upper and

lower shear boxes can be significant and lead to unconservative curvature of the critical portion of the FSS strength envelope. This frequently occurs at low normal stresses because the weak specimen cannot maintain the gap and tends to tilt during shear, which is unfortunate because the FSS at low effective normal stresses is important for compacted embankments.

Additionally, the large thickness of the DS specimen relative to a RS specimen leads to dramatically longer times for specimen consolidation and drained shearing. The time spent consolidating a reconstituted specimens for a FSS DS test can be excessive because new material has to be added to the specimen so there is sufficient soil in the top shear box before shearing commences. In addition, the shear displacement rate required for full drainage during direct shear is usually at least an order of magnitude slower than for a RS test. For example, Eagle Ford Shale, a high plasticity clay, requires a shear displacement rate for full drainage of 0.0008 mm/min and 0.018 mm/min for DS and RS testing, respectively. Therefore, Stark and Eid (1997) did not recommend the DS for FSS testing and developed a conversion factor for RS measured values to the CD-TX mode of shear.

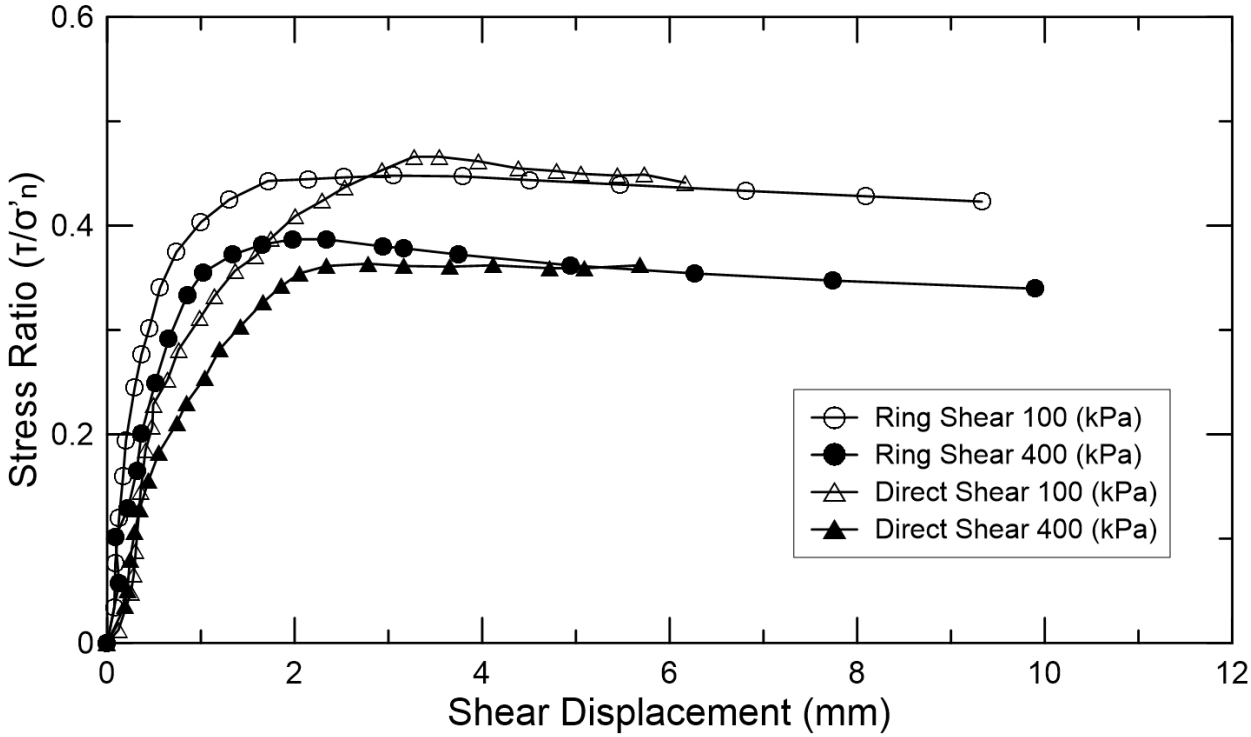

Figure 5 Shear stress ratio versus shear displacement for direct shear and ring shear tests on Panoche Shale from Eid (1996).

(b) <u>Comparison of RS and DS FSS Test Results</u>

To further investigate the values of FSS measured using RS and DS devices, DS tests were conducted herein on soils that had already been tested in RS. In particular, at least two soils from each of the three CF groups in the FSS correlation in **Figure 2** were tested to augment the comparison of RS and DS values of FSS started by Eid (1996). All of the measured shear stress-shear displacement relationships for the RS and DS tests on the soils from each CF group are presented in **Appendix B**. The resulting FSS strength envelopes obtained from the RS and DS devices for the CF groups: CF ≤ 20% (Duck Creek Shale), 25 ≤ CF ≤ 45% (NoVA Clay), and CF ≥ 50% (brown London Clay) are presented in **Figure 6, Figure 7,** and **Figure 8**, respectively. The

FSS strength envelopes for the other three comparisons for CF groups: 20% ≤ CF (Urbana Till), 25 ≤ CF ≤ 45% (Pierre Shale) and CF ≤ 50% (Eagle Ford Shale) are shown in **Appendix C**. As expected, the DS and RS devices yield similar FSS strength envelopes regardless of the CF group because the mode of consolidation and shear are similar. This reaffirms the data and conclusion generated by Eid (1996).

In particular, **Figure 6** presents the various strength envelopes for Duck Creek Shale (CF ≤ 20%). As expected, the RS and DS derived strength envelopes are similar. In addition, the RS and DS strength envelopes plot below the FSS correlation in **Figure 2**, which is in excellent agreement with the RS envelope after it was reduced by 2.5° (blue triangles). This is expected because RS and DS devices fail the specimens along a nearly horizontal surface so the resulting values of FSS should fall below the FSS correlation in **Figure 2**, which corresponds to a CD-TX mode of shear. Conversely, the DS strength envelope even plots below the FSS correlation after reducing it by 2.5°, probably due to progressive failure in the normally consolidated specimen, soil extrusion, and/or other problems with DS testing that are mentioned above. A similar comparison and result is presented in **Appendix C** for Urbana Till, which is also in the lowest CF Group (20%).

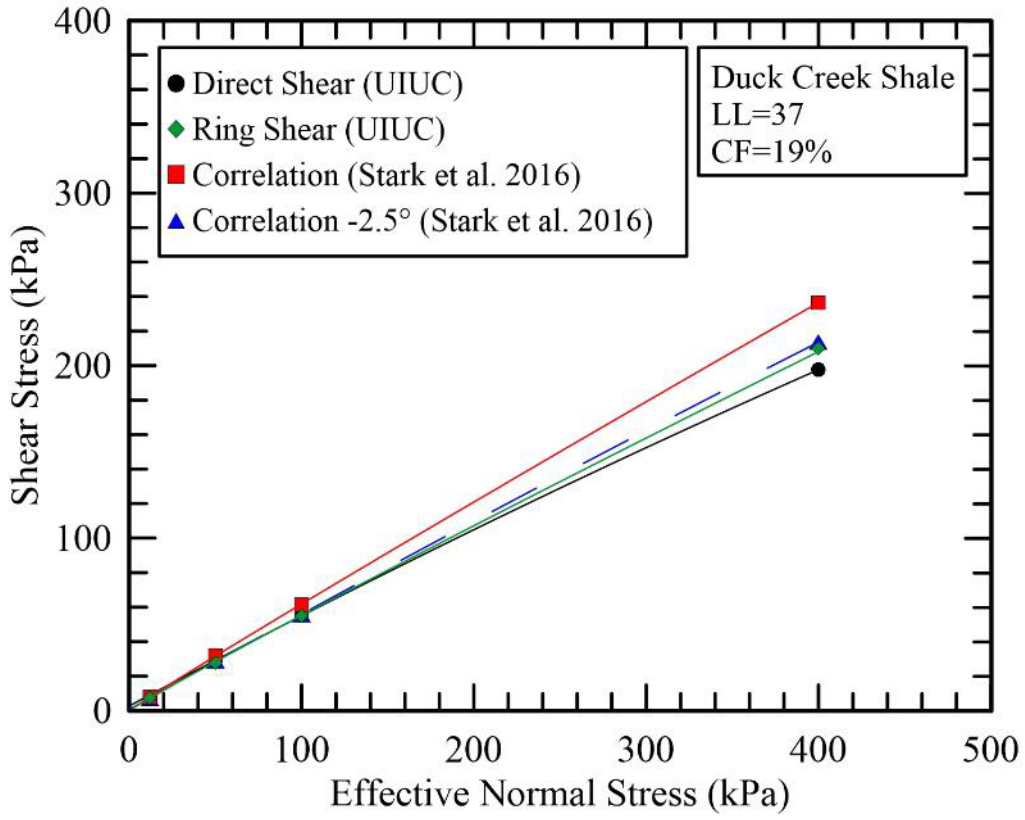

Figure 6: FSS strength envelopes from RS and DS testing on Duck Creek Shale and FSS empirical correlation for CF group ≤ 20%.

Figure 7 presents the various strength envelopes for Pierre Shale (25% ≤ CF ≤ 45%). As expected, the RS and DS derived strength envelopes are in agreement and plot below the FSS correlation in **Figure 2**. The RS and DS derived strength envelopes are also in agreement with the correlation after it was reduced by 2.5° (blue triangles). A similar comparison and result is presented in **Appendix C** for a split-sample of the NoVA Clay tested by Castellanos (2014) that was provided to the first author for comparison testing before Castellanos (2014) completed his testing. The results for NoVA Clay (25%≤ CF ≤ 45%) are similar to those shown in **Figure 7** for Pierre Shale.

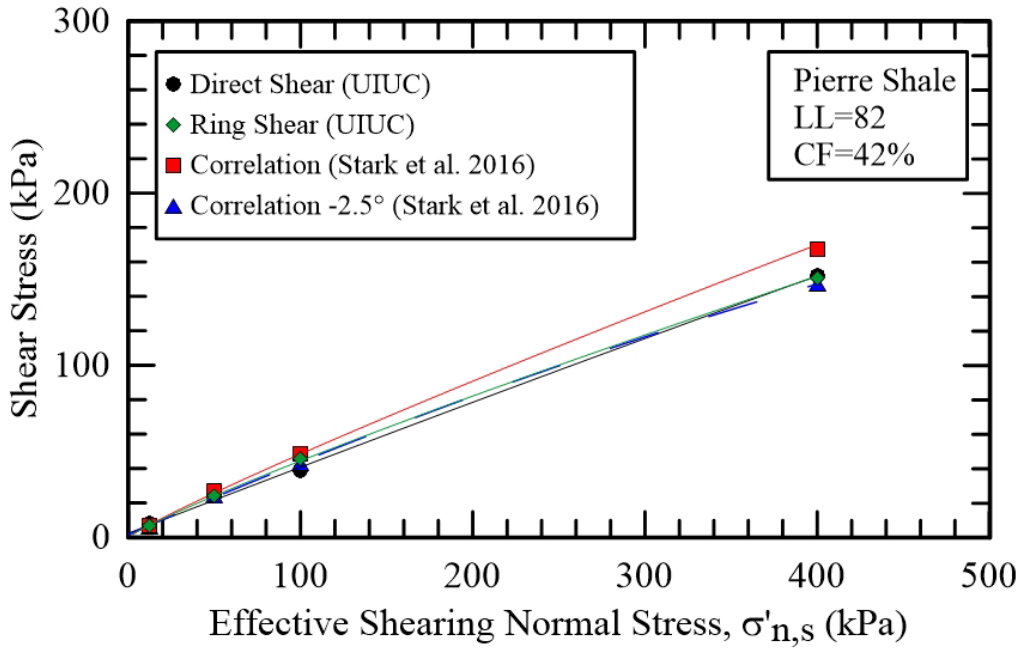

Figure 7: FSS strength envelopes from RS and DS testing on Pierre Shale and FSS empirical correlation for CF group 25% ≤ CF ≤ 45%.

Figure 8 presents the various strength envelopes for brown London Clay, which falls in the highest CF Group (CF ≥ 50%). Skempton (1977) focused on brown London Clay from Chandler and Skempton (1974) with a LL, plastic limit (PL), and a CF of 82, 30, and 55, respectively. In this study, brown London Clay from Bradwell, England was tested and has a LL, PL, and CF of 101, 30, and 66, respectively, so the material is more plastic than the brown London Clay considered by Skempton (1977).

The RS and DS strength envelopes again plot below the Stark and Eid (1997) FSS correlation. However, the RS and DS shear strength envelopes are in agreement with the FSS correlation in **Figure 2** after the FSS friction angles are reduced by 2.5°. A similar comparison and result is presented in **Appendix C** for Eagle Ford Shale with a CF ≥ 50%.

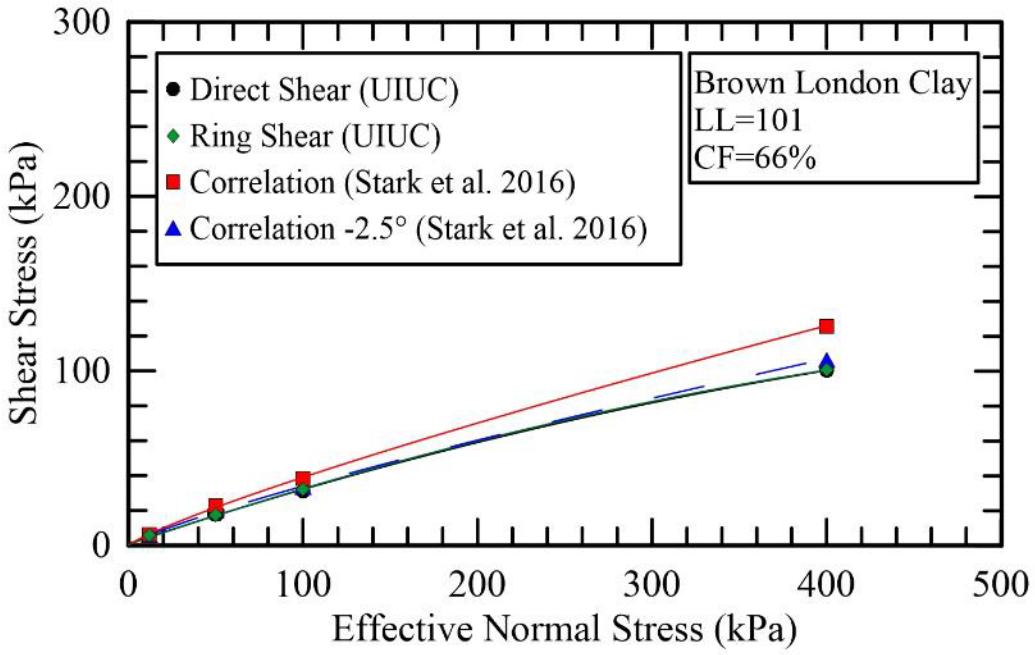

Figure 8: FSS strength envelopes from RS and DS testing on brown London Clay and FSS empirical correlation for CF group $\geq$ 50%.

In summary, RS and DS devices yield similar FSS strength envelopes for the three CF groups used in the FSS correlation in **Figure 2** if the testing is performed correctly (see Stark, 2017). Therefore, the strength envelopes determined from RS and DS testing should plot in between the FSS and residual strength correlations presented in Stark and Eid (1997). If a DS derived strength envelope is in agreement with the FSS correlation in **Figure 2**, e.g., Castellanos et al. (2016), the data is incorrect because the DS mode of shear and testing conditions are different than CD TX. In fact, Osano (2012) shows that the DS device yields lower values than the RS device, which also contradicts Castellanos et al. (2016). Given that Castellanos et al. (2016) present values of FSS derived from RS testing that are lower than the drained residual strength estimated from the empirical correlation described below (see Stark, 2017), their data and conclusions about RS and DS testing should be dismissed. Castellanos (2014) and Castellanos et al. (2013) used the original porous discs provided by the manufacturer of the Bromhead ring shear device to perform their RS

tests. These porous discs have insufficient serration, which leads to FSS envelopes that significantly underestimates the FSS because the porous disc slides over the surface of the soil specimen instead of penetrating the soil to cause shearing within the soil. The serration pattern proposed by Stark and Eid (1993) allows for sufficient interlocking between the upper porous disc and the normally consolidated soil to effectively shear the soil and yield an accurate measurement of the FSS. This observation is emphasized in the Closure (Eid and Rabie, 2018) to Eid and Rabie (2017).

Eid (1996) also shows that the RS and DS devices yielded similar values of FSS and the DS FSSs are less than the CD-TX device. For example, the CD-TX tests on Panoche shale performed by Eid (1996) are shown in **Figure 5** and used to estimate the CD-TX secant FSS friction angles shown in **Table 3**, where the DS secant FSS friction angles are less than the CD-TX values. **Table 3** shows the RS and DS devices yield similar secant FSS friction angles, which are less than CD-TX by about 2.5° for a large range of effective normal stress. This reinforces the recommendation to increase the RS values of FSS by 2.5°. This is also confirmed by Duncan et al. (2014) on page 74, which states that triaxial compression tests produced higher friction angles than direct shear tests.

Table 3. Secant FSS friction angles from RS, DS, and CD triaxial compression tests on Panoche Shale from Eid (1996).

Effective Normal Stress (kPa)	Ring Shear Secant FSS Friction Angle (degrees)	Direct Shear Secant FSS Friction Angle (degrees)	CD Triaxial Compression Secant FSS Friction Angle (degrees)
100	24.2º	24.7º	26.2º
400	21.2º	20.0º	22.8º

FSS EMPIRICAL CORRELATIONS

Six (6) main correlations have been published to estimate the FSS envelope primarily using RS data and the FSS correlation in Stark and Eid (1997). The other five (5) correlations are presented by Mesri and Shahien (2003), Wright (2005), Eid and Rabie (2017), and Castellanos (2014) or Castellanos et al. (2016). Wright (2005) only presents a correlation for high plasticity and high CF fine-grained soils so it is included in only the third CF group comparison because these soils are most susceptible to strength loss due to wet-dry cycles in compacted highway embankments. All of these FSS correlations conclude that the FSS envelope is stress dependent, which is now accepted by many practitioners.

The main uses of non site-specific empirical correlations, particularly the one shown in **Figure 2**, are: (1) verification of laboratory shear test results, (2) evaluation of potential borrow sources, and (3) planning level design. Empirical correlations should not be used for final design unless site specific shear testing confirms the empirical correlation is applicable to the soils present at the project site. This paper also discusses selecting appropriate correlation parameters and "anchoring" FSS correlations using site specific shear testing before undertaking final design.

These six (6) empirical FSS correlations are compared using two soils from each CF group. In other words, the index properties for two soils from each CF group in **Table A-1** are used to estimate the FSS strength envelope using each correlation and the resulting FSS envelopes are compared in a single graph to illustrate the usefulness of these correlations. Two soils are selected from each CF group that exhibit a large difference in plasticity and CF to test the range of the FSS

correlations. For example, Duck Creek Shale (LL=37, PI=12, and CF=19%) and San Francisco Bay Mud (LL=76, PI=35, and CF=16%) are used to compare the five (5) available FSS empirical correlations for the first CF group (CF≤20%).

Figure 9 presents the comparison of FSS correlations for values of CF≤ 20% and shows there is good agreement between the five (5) available correlations for Duck Creek Shale at the low plasticity end of this CF group (see solid lines). However, the Castellanos (2014) correlation based on PI in percent yields a significantly lower FSS envelope for San Francisco Bay Mud (see dashed lines), which is just a little higher than the drained residual strength correlation in Stark and Hussain (2013) and confirms this correlation is incorrect. As expected, the correlations by Stark and Eid (1997), Mesri and Shahien (2003), and Eid and Rabie (2017) yield similar FSS envelopes because they are based on the same database of RS test results.

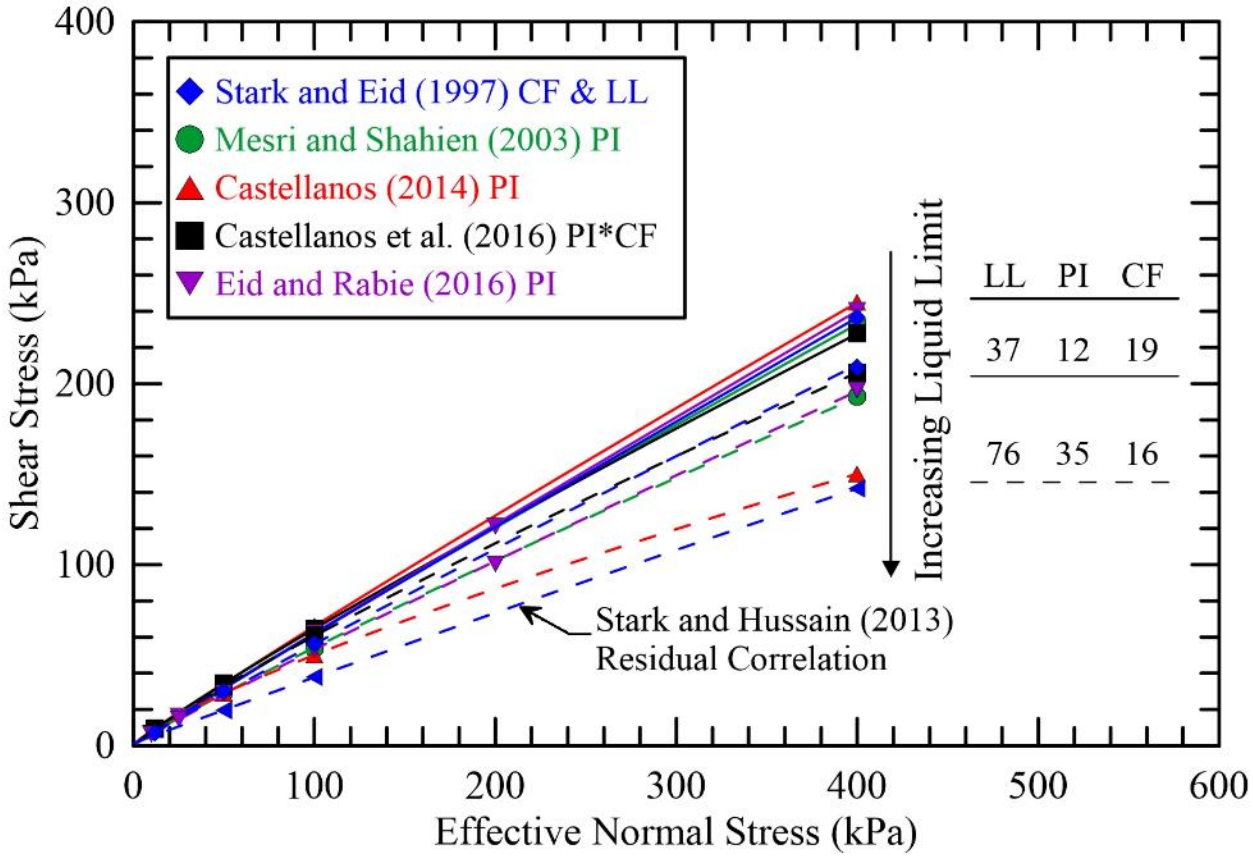

Figure 9: FSS strength envelopes from five (5) empirical correlations for Duck Creek Shale and San Francisco Bay Mud for CF ≤ 20%.

Figure 10 uses Oso Landslide Lacustrine Clay (LL=38, PI=17, and CF=31) and Bearpaw Shale (LL=128, PI=101, and CF=43) to compare the empirical correlations for the second CF group (25% ≤ CF ≤ 45%). **Figure 10** presents the comparison of FSS correlations for values of 25% ≤ CF ≤ 45% and shows there is again good agreement between the five (5) available correlations for the low plasticity soil, i.e., Oso Landslide Lacustrine Clay (see solid lines), but not for the high plasticity soil (Bearpaw Shale) in the middle CF group. For Bearpaw Shale, the Castellanos et al. (2016) correlation based on PI*CF in percent yields a significantly lower FSS envelope (see dashed lines) than the other correlations. This correlation uses PI*CF, both in percent, to correlate

with FSS instead of PI in percent as used by Castellanos (2014). This correlation is similar to the CALIP parameter proposed by Collota et al. (1989) for drained residual strength, which is defined as CF^2*LL*PI*10-5. In addition, comparing **Figure 9** and **Figure 10** shows that the two (2) correlations by Castellanos (2014), i.e., PI and PI*CF, are good for one CF group and bad for another so neither of the correlations is reliable for a range of soils and neither should be used.

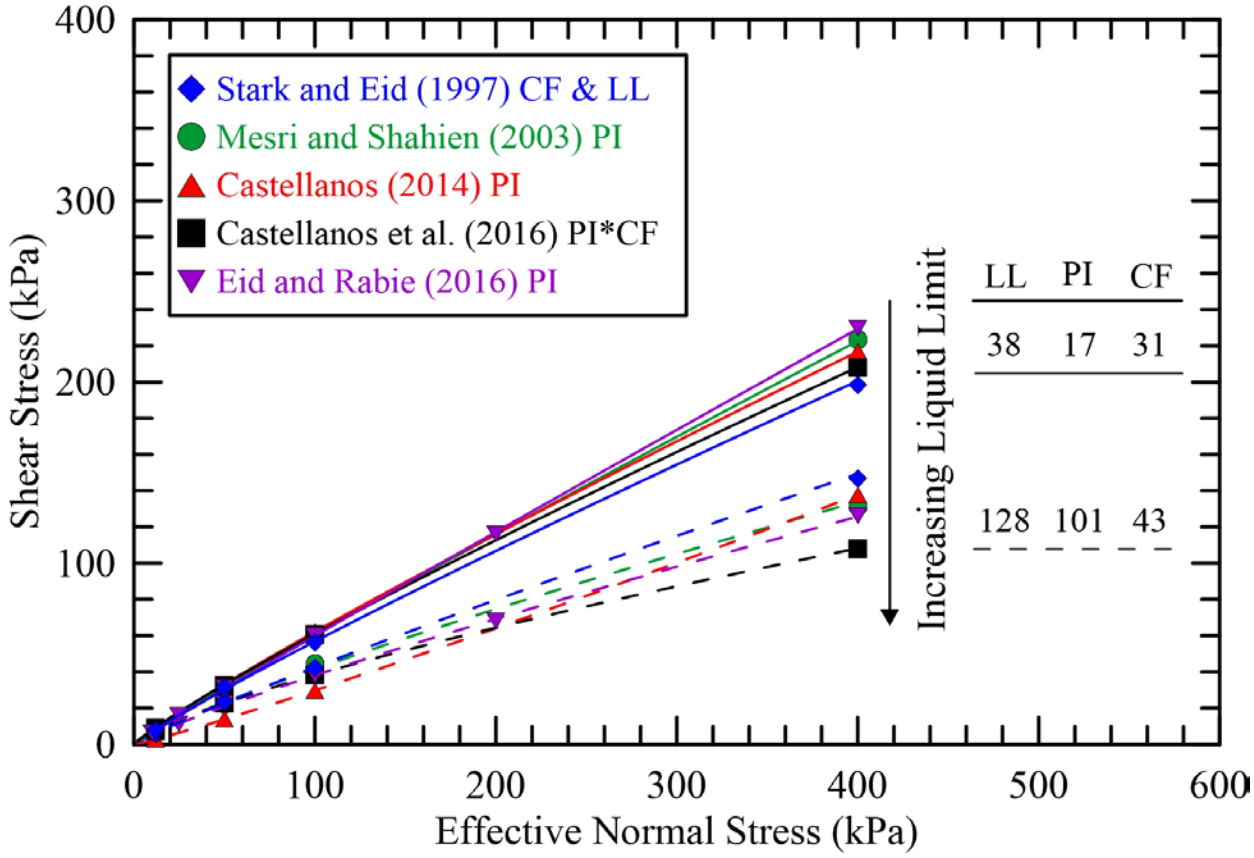

Figure 10: FSS strength envelopes from five (5) empirical correlations for Oso Lacustrine Clay and Bearpaw Shale for CF 25% ≤ CF ≤ 45%.

Finally, **Figure 11** uses claystone from Big Bear, California (LL=74, PI=52, and CF=54) and Pierre Shale (LL=184, PI=129, and CF=84) to compare the empirical FSS correlations for the third or highest CF group (CF≥50%). The FSS correlation by Wright (2005) is included in

Figure 11 because it presents a correlation for high plasticity fine-grained soils that was the focus of his study on compacted highway embankments.

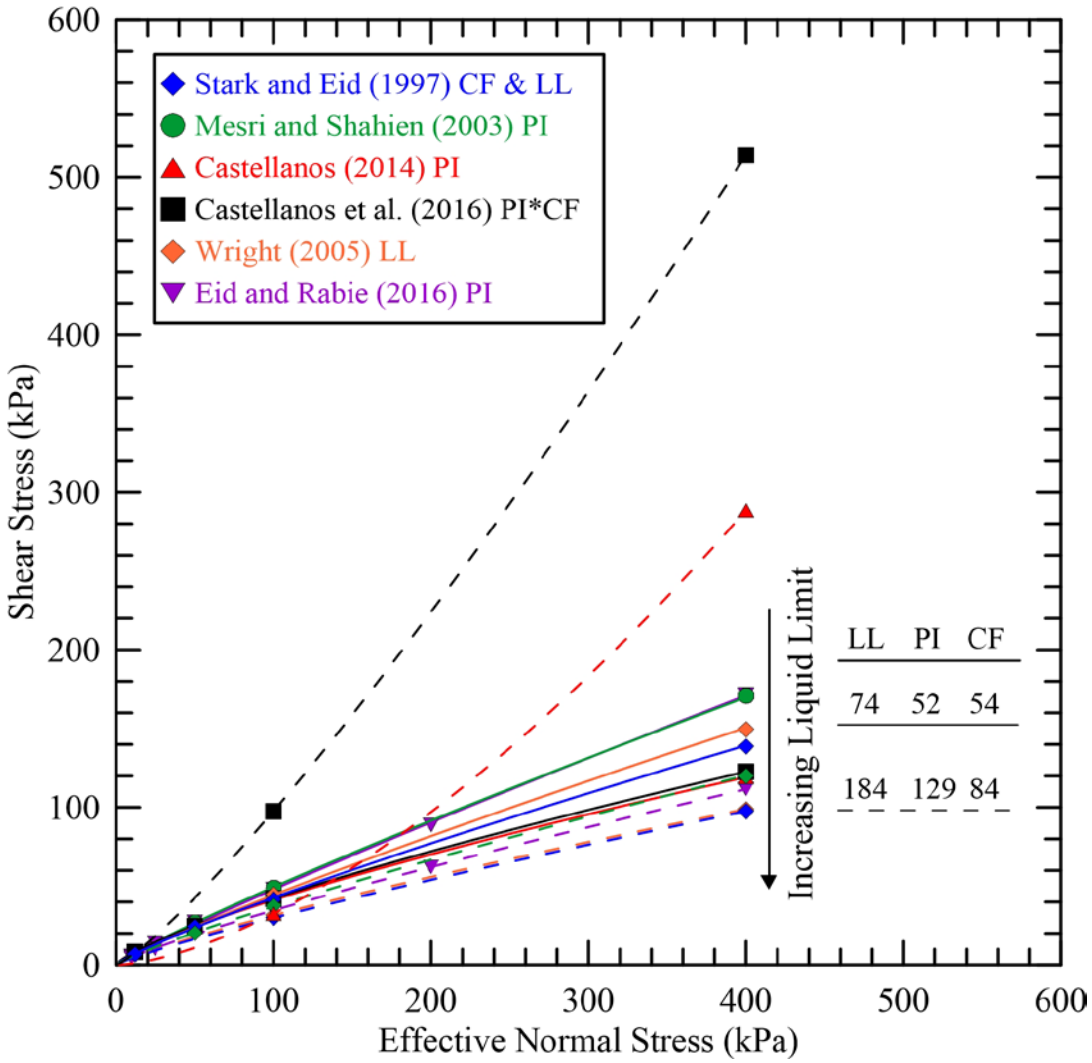

Figure 11: FSS strength envelopes from six (6) empirical correlations for Big Bear Claystone and Pierre Shale for CF $\geq$ 50%.

Figure 11 presents the comparison of FSS correlations for values of CF $\geq$50% and shows there is considerable scatter and disagreement between the six (6) available FSS correlations even for the lower plasticity soil, i.e., Big Bear Claystone (see solid lines) in this CF group. This is unfortunate

because high plasticity and high CF soils are most susceptible to softening in natural and compacted slopes and most likely to develop a FSS condition in the field. For the low plasticity soil in CF Group #3 (Big Bear Claystone), the Mesri and Shahien (2014) correlation yields a slightly higher FSS envelope than the FSS correlation in **Figure 2** but it is still in good agreement.

For the high plasticity soil in CF Group #3 (Pierre Shale), both the Castellanos et al. (2016) and Castellanos (2014) correlations blow-up and yield unreasonably high FSS envelopes (see dashed lines). For example, these correlations yield FSS secant fraction angles of 35 and 52 degrees at an effective normal stress of 400 kPa, respectively, which are too high for a normally consolidated specimen. In particular, these two correlations blow-up and yield unreasonable FSS envelopes at a PI > 70 for a normal effective stress of 400 kPa. Therefore, the Castellanos et al. (2016) and Castellanos (2014) correlations should not be used for soils with a PI > 70. This is unfortunate because high plasticity and high CF soils are most susceptible to developing a FSS condition. As expected, the correlations by Stark and Eid (1997) and Wright (2005) yield similar FSS envelopes for the high CF Group because they are based on the same FSS RS database. The Mesri and Shahien (2014) and Eid and Rabie (2017) correlations yielded slightly higher FSS envelopes than the FSS correlation in **Figure 2** but well below the unreasonable FSS envelopes from the Castellanos et al. (2016) and Castellanos (2014) correlations.

POWER FUNCTION TO CREATE FSS STRENGTH ENVELOPE

The stress-dependent FSS envelope also can be modeled using a power function as suggested by Mesri and Shahein (2003) and Lade (2010) and shown below:

583 $$\boldsymbol{FSS} = a \times P_a \times \left(\frac{\sigma'_n}{P_a}\right)^b \quad \textbf{(1)}$$

584

585 where “a” and “b” are dimensionless coefficients that control the scale and curvature of the
586 strength envelope, respectively; σ'_n is the effective normal stress; FSS is the fully softened shear
587 strength; and P_a is the atmospheric pressure in the same units as FSS and σ'_n (Lade 2010).

588

589 **Figure 12** presents values of *a* and *b* that can be used to predict the FSS strength envelopes for the
590 three CF groups (CF ≤ 20%, 25% ≤ CF ≤ 45%, and CF ≥ 50%) in the FSS correlation shown in
591 **Figure 2**. The coefficients *a* and *b* can be used with **Eq. (1)** to plot the stress-dependent FSS
592 envelope using more than the five effective normal stresses (including zero) used in the FSS
593 correlation in **Figure 2**.

594

595 **Figure 12** shows the power function coefficient *b* has little influence on the FSS power function
596 so the average values for each CF group can be used without significantly compromising the
597 resulting strength envelope. For example, average values of *b* from **Figure 12** are: 0.960, 0.905,
598 and 0.852 for CF groups of: CF ≤ 20%, 25 ≤ CF ≤ 45%, and CF ≥ 50%, respectively. However,
599 there is variability and influence of the *a* coefficient on the FSS envelope. Therefore, the current
600 study developed a mathematical expression for each trend line for the *a* coefficient, which can be
601 used with the power function to estimate the FSS strength envelope. A linear expression adequately
602 represents the variability of the FSS *a* coefficient as a function of liquid limit (LL) for each one of
603 the CF groups as shown below:

604

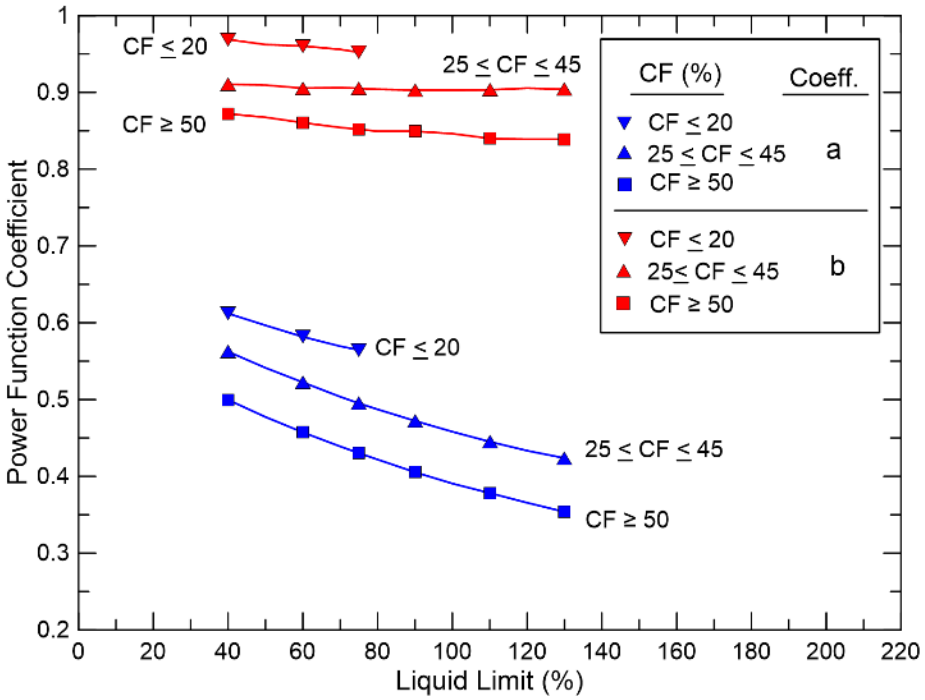

Figure 12: Recommended power function coefficients "a" and "b" to estimate drained FSS envelopes for the three CF groups as a function of LL.

Fully Softened Strength "a" coefficients:

CF ≤ 20%: $a_{FSS} = -0.0014(LL) + 0.6656$ **(2)**

25% ≤ CF ≤ 45%: $a_{FSS} = -0.0015(LL) + 0.6149$ **(3)**

CF ≥ 50%: $a_{FSS} = -0.0016(LL) + 0.5546$ **(4)**

The FSS mathematical expressions developed are in good agreement with the trend lines in the FSS correlation presented in **Figure 2** for the full range of LL values. The values of LL and CF used in the equations should be in terms of whole numbers not decimal form. This can be easily investigated using an EXCEL spreadsheet developed herein that includes the equations for the FSS trend lines (see **Appendix D**) and a power function with the values of *a* and *b* coefficient shown

in **Figure 12**. The equations for the drained residual strength trend lines included in this EXCEL spreadsheet are shown in **Appendix E**. The EXCEL spreadsheet that incorporates both the FSS and residual strength correlations is available at **www.tstark.net** and can be used and distributed throughout the geotechnical profession.

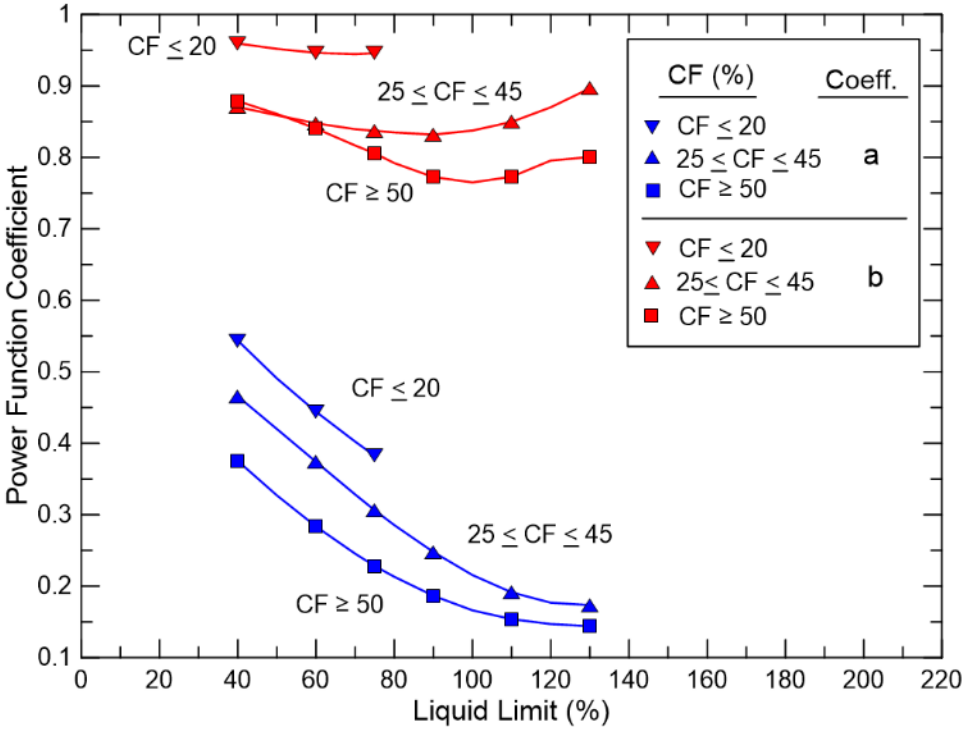

Figure 13: Recommended power function coefficients "a" and "b" to estimate drained residual strength envelopes for the three CF groups as a function of LL.

Power function coefficients were also developed for the residual strength correlation presented in Stark and Hussain (2013). The mathematical expressions for *a* and *b* to represent the trend lines in the residual strength correlation using a power function were developed using the data in **Figure 13**. The quadratic expressions shown below adequately represent the variability of coefficients *a* and *b* as a function of liquid limit (LL) for each one of the CF groups shown in **Figure 13**:

Residual Strength "a" coefficients:

CF ≤ 20%: $a_r = 3*10^{-5}(LL)^2 - 0.0080(LL) + 0.8047$ **(5)**

25% ≤ CF ≤ 45%: $a_r = 3*10^{-5}(LL)^2 - 0.0076(LL) + 0.7448$ **(6)**

CF ≥ 50%: $a_r = 3*10^{-5}(LL)^2 - 0.0077(LL) + 0.6352$ **(7)**

Residual Strength "b" coefficients:

CF ≤ 20%: $b_r = 2*10^{-5}(LL)^2 - 0.0023(LL) + 1.0261$ **(8)**

25% ≤ CF ≤ 45%: $b_r = 2*10^{-5}(LL)^2 - 0.0050(LL) + 0.997$ **(9)**

CF ≥ 50%: $b_r = 3*10^{-5}(LL)^2 - 0.0059(LL) + 1.0792$ **(10)**

The residual strength mathematical expressions presented above also can be compared with the power function and the values of *a* and *b* coefficient shown in **Figure 13** using the spreadsheet mentioned above. There is less agreement between the drained residual strength trend line equations and the power function coefficients but the difference is small for planning level investigations if it is desired to use a drained residual strength envelope from the power function instead of the empirical correlation.

APPLICATION OF FSS EMPIRICAL CORRLEATION TO SAN LUIS DAM

Using a DS apparatus, Stark and Duncan (1991) show that the slopewash involved in the 1981 upstream slope failure of San Luis Dam (now known as B.F. Sisk Dam) in 1981 exhibits a fairly

linear FSS strength envelope at effective normal stresses above the preconsolidation pressure (see **Figure 14**). The drained residual strength envelope for the upstream slopewash is also fairly linear. This testing was performed between 1986 and 1987 before the stress-dependent nature of the drained FSS and residual strength envelopes was reported in Stark and Eid (1994). However, this case history provides an opportunity to assess the accuracy of the FSS and residual empirical correlations presented herein.

Two (2) block samples of the upstream slopewash were provided by the U.S. Bureau of Reclamation with average LL and CF 66 (60 to 72) and 63% and 40 (37 to 43) and 34%. Testing was primarily conducted on the second block sample with a CF of 34%, so the slopewash falls into the transitional shear or middle CF group. One of the desiccated downstream slopewash block samples had a similar average LL and CF of 42 (38 to 45) and 35%, respectively. The other desiccated downstream slopewash block sample exhibited a higher plasticity with the average LL and CF being 66 (60 to 72) and 63%, respectively, so this downstream slopewash sample falls into the sliding shear or third CF group.

There was little difference between the peak shearing resistances of undisturbed and reconstituted specimens (c' = 0 psf and ϕ' = 25°) of the upstream slopewash at effective normal stresses greater than 144 kPa (3,000 psf) because the slopewash had been wetted by the reservoir and the matric suction pressures in the desiccated soil had been removed resulting in essentially a normally consolidated material. Only at effective normal stresses below about 144 kPa (3,000 psf) did the undisturbed DS specimens exhibit slightly higher peak strengths, which is indicative of a slightly

overconsolidated material. The residual strengths of undisturbed and reconstituted specimens of the upstream slopewash were also the same (c_r' = 0 psf and ϕ_r' = 15°).

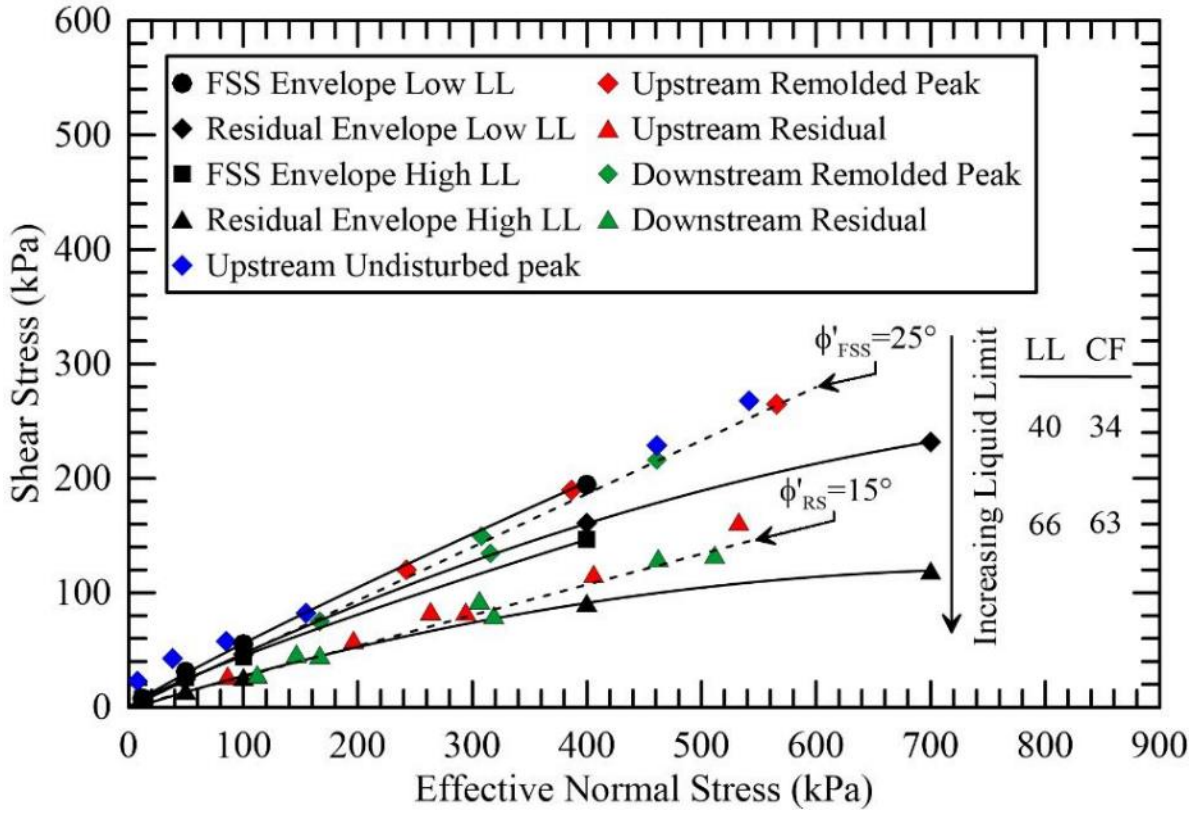

Figure 14: Measured and estimated drained FSS and residual strength envelopes for upstream and downstream slopewash at San Luis Dam.

Stark et al. (2014) calculate the FS of the upstream slope at different operational stages using a failure surface that remains in the slopewash to the slope toe after passing through the Zone 1 (impervious core) material (see **Table 4** for FS values). These slope stability analyses were augmented herein to determine if the FSS and residual correlations presented herein would have accurately predicted the stability of the upstream slope.

Table 4. Summary of factor of safety for upstream slope of San Luis Dam.

Reservoir Condition and Slopewash Shear Strength	Stark and Duncan (1991) (Linear Strength Envelopes)	Present Study (Linear FSS and Residual Strength Envelopes using LL = 42 and CF = 34%)	Present Study (Stress Dependent FSS and Residual Strength Envelopes using LL = 42 and CF = 34%)	Present Study (Stress Dependent FSS and Residual Strength Envelopes using LL = 66 and CF = 63%)
End of construction & Desiccated slopewash: (c' = 263 kPa, $\phi' = 39^0$)	4.8	4.7	4.7	4.7
Reservoir Full & FSS: (c' = 0 kPa, $\phi'_{FSS} = 25^0$)	2.0	1.9	1.9	1.7
Reservoir Down & FSS: (c' = 0 kPa, $\phi'_{FSS} = 25^0$)	1.3	1.5	1.6	1.2
Reservoir Down & Residual: (c' = 0 kPa, $\phi'_r = 15^0$)	0.9	1.05	1.13	0.86

The stress-dependent FSS envelope for the upstream slopewash yields a slightly higher FS (1.6) than the linear FSS envelope (1.5) using a LL of 42 and CF = 34%. These values of FS are higher than the FS (1.3) obtained using the linear FSS envelope ($\phi'_{FSS} = 25^0$) in Stark and Duncan (1991). This difference in FS is due to the stress-dependent FSS envelope being higher at low effective normal stresses than the linear strength envelope of $\phi'_{FSS} = 25^0$ (see **Figure 14**). For comparison

purposes, the FSS secant friction angle for the stress-dependent FSS envelope ranges from 33.5 to 26.0 degrees so the empirical correlation yields a strength envelope that is greater than the linear FSS strength envelope of 25^0 from Stark and Duncan (1991) for the full range of effective normal stresses.

The largest difference in FS for the upstream slope involves the drained residual strength. The stress-dependent residual envelope is significantly higher than the linear envelope ($\phi'_r = 15^0$) (see **Figure 14**). As a result, the stress-dependent residual envelope yielded a FS (1.13) greater than unity (1.0), which is not indicative of slope instability for the pore-water pressure used in the analysis. For comparison, the secant friction angle for the stress-dependent residual strength envelope ranges from 26.1 to 18.6 degrees so the empirical correlation yields a strength envelope that is greater than the linear envelope of 15^0 for the full range of effective normal stresses. The linear residual strength envelope ($\phi'_r = 15^0$) was measured by the first author using many travels in a reversal direct shear test and a pre-cut specimen. The laborious and time-consuming procedure lead the first author to pursue development of a torsional ring shear device and test procedure to effectively measure the drained residual strength. However, the drained residual strength of the high plasticity slopewash (LL=66) provides a FS below unity as discussed below.

The stress-dependent FSS envelope for the high plasticity (LL=66) downstream slopewash yields a lower FS (1.7) than the linear envelope (1.9). This low FS is due to the stress-dependent FSS envelope being lower than the linear strength envelope of $\phi'_{FSS} = 25^0$ (see **Figure 14**) due the higher plasticity and a CF that exceeds 50% so it falls in the highest CF group. For comparison purposes, the secant friction angle for the stress-dependent FSS envelope ranges from 30.8 to 20.1

degrees so the empirical correlation yields a strength envelope that is lower than the linear envelope ($\phi'_{FSS} = 25^0$) at higher effective normal stresses. The stress-dependent residual strength envelope is also significantly lower than the linear envelope ($\phi'_r = 15^0$) (see **Table 4**) and ranges from 16.0 to 9.7 degrees. As a result, the stress-dependent residual envelope yielded a FS (0.86), which is significantly lower than unity (1.0). This block sample was obtained from downstream of the slide and may not be representative of all of the slopewash involved in the upstream slope failure.

In summary, the FSS and residual strength correlations updated herein provide a reasonable inverse analysis of the upstream slope failure in San Luis Dam. In general, if a FSS was mobilized at the 1981 drawdown level the slope would have been stable and if a drained residual strength was mobilized it would have been unstable to marginally stable based on the pore-water pressures used in the analysis. This provides some reassurance that the correlations provide reasonable FSS and residual strength envelopes but should be verified for final design as discussed below.

SELECTING INPUT PARAMETERS FOR EMPIRICAL CORRELATIONS

Because the FSS correlation in **Figure 2** is used in practice, there has been debate about the appropriate values of LL and CF to use with the correlations. The following two scenarios have been used in practice:

1. Using numerical average values of LL and CF because the deposit fill is uniform, i.e., a weak layer or bedding is unlikely so the material is adequately represented by a limited number of samples and borings.

2. Using one standard deviation above the mean values of LL and CF because there is a likelihood that a weak layer or bedding is present given limited subsurface information. Average values of LL and CF are usually lower than values for the weakest layer because there is more data for the materials outside than inside the weak layer.

Instead of using numerical statistics and the two scenarios above, it is recommended herein that the LL and CF be plotted using histograms. This approach is recommended because statistics can be skewed by some low values that probably will not control slope or retaining wall stability. **Table 5** presents values of LL and CF for a heavily over-consolidated clay near Seattle, Washington, which are plotted in histograms in **Figure 15**. **Figure 15** presents 192 values of LL and CF from the entire project area. CF is an important parameter because it determines which type of shearing behavior the soil will exhibit. There is an important difference between the average and average plus one standard deviation values of CF (40 and 62) because it shifts the clay into the highest CF group instead of the middle CF group.

Figure 15(a) shows that the average value of LL is skewed downward to 60 (see **Table 5**) because the histogram shows a lot of LL values from 60 to 85. Therefore, a LL value of 70 is reasonable to estimate the FSS at this site instead of the numerical average LL of 60. This is a significant difference in LL because the slope of the trend lines is steep in this range of LL. **Figure 15(b)**

779 also shows a representative value of CF is 51 or greater than 50% (highest CF group), for
780 estimating the FSS instead of the average value of 40% (middle CF group). The value of CF is
781 not important once it exceeds 50% so many designers simply use 50% and vary the LL for planning
782 level decisions.

783

784

785 **Table 5.** Summary of LL and CF for a project site involving a mechanically
786 overconsolidated clay.

Material Type or Location	Minimum and Maximum LL (%)	LL Average, Median, and Standard Deviation	Minimum and Maximum CF (%)	CF Average, Median, and Standard Deviation	Planning Design LL based on Histogram	Planning Design CF based on Histogram*
Across site	22/92	60/64/16	2/81	40/43/22	70	55/>50%
Particular slope	30/83	55/47/21	4/81	43/55/31	75	55/>50%

787 **NOTE:**
788 * Use CF >50% for recommended strength values
789
790
791
792

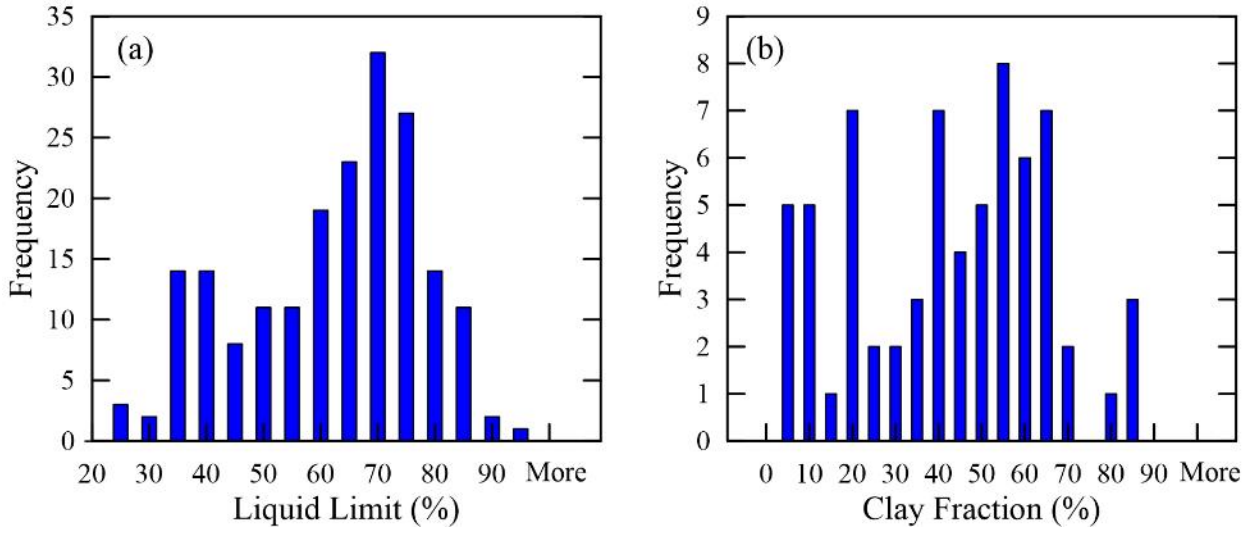

793
794 **Figure 15:** Histograms of: (a) LL and (b) CF for heavily over-consolidated clay project site.

Figure 16 presents the LL and CF values for one slope of interest within the large Seattle project described above (see **Figure 15**). **Figure 16** presents twenty-one (21) values of LL and CF instead of the 192 values from the entire project shown in **Figure 15**. **Table 5** also presents values of LL and CF for this particular slope. The histograms of LL and CF in **Figure 16(a)** and **(b)**, respectively, indicate there are two types of soil in this slope. One soil type has a LL ranging from 30 to 50 while the other has a LL ranging from 70 to 85. This distinct separation in LL values indicates the presence of a low plasticity (higher strength) and a high plasticity (lower strength) soil within the slope. For slope stability purposes, the soil with a higher LL will control stability because the critical failure surface will be minimized in the stronger materials. One soil type has a CF less than 45% while the other soil ranges from 55 to 85%. Clearly the soil with a CF greater than 50% will control the stability of the slope and should be used with the corresponding LL. Therefore, the FSS envelope for this particular slope should be estimated using a value of LL of 75 with a range of 70 to 85 and a CF greater than 50% and not the average CF of only 43.

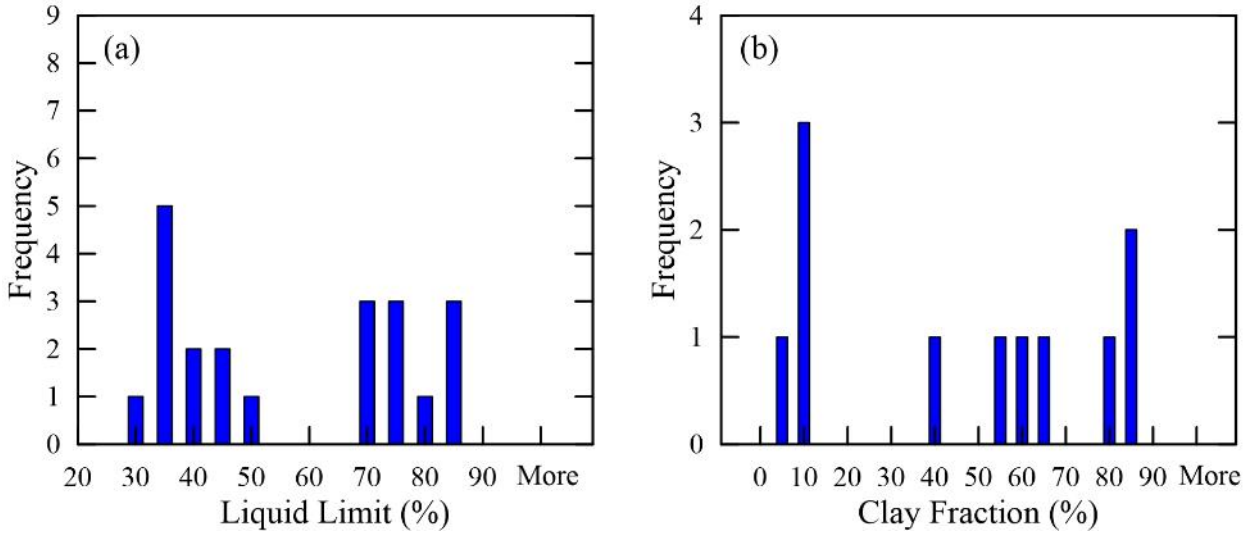

Figure 16: Histograms of: (a) LL and (b) CF for a particular slope in the heavily over-consolidated clay in the project site shown in **Figure 15**.

In summary, the highest grouping of slope-specific values of LL and CF in a histogram should be used to estimate the FSS and residual strength envelopes instead of some form of numerical average. The resulting strength envelopes can be used to verify laboratory shear test results, evaluate potential borrow sources, and planning level design for this slope.

ANCHORING FSS CORRELATIONS

Over large areas, it is desirable to estimate the range of shear strength based on index properties, such as LL and CF, because it is impractical to perform shear tests on all of the relevant materials. If a wide range of soils is considered as potential borrow material, at least one soil from each CF group should be tested to ensure reasonable agreement with the strength envelopes estimated from the empirical trend lines and/or power function coefficients. The FSS empirical correlation and power function coefficients are based on a finite number of soils (60) that may not include any soils from the site of interest. Hence, the correlation should be calibrated to ensure project specific soils are in agreement before it is used for final design.

For example, it was desirable to estimate the range of the FSS using index properties, such as LL and CF, for the Dallas Floodway because it was not practical to perform shear tests on all of the relevant materials over the 38.4 km of levee being investigated (Gamez and Stark, 2014). Calibrating the empirical correlation to ensure project specific soils are in agreement with the correlation was desired before the correlation could considered for final design purposes. Because most of the observed slope failures along the approximately 38.4 km of levee system are of shallow

to intermediate depth, most of the direct shear testing (Stephens et al., 2011) and anchoring with the FSS correlation in **Figure 2** occurred at effective normal stresses of 50 and 100 kPa.

Figure 17 shows the LL and CF histograms of thirty-one (31) samples of the levee materials in the slope instability areas along the floodway. The thirty-one (31) samples exhibit LL ranging from 35 to 93 and these samples were used to measure the FSS as discussed below. The numerical average LL is about 77 for the range of samples tested and the majority of the CF values exceed 50%. From the histograms, a design value of LL is 80 and a CF greater than 50% is recommended. Stephens et al. (2011) present direct shear test results on these thirty-one (31) soils and the values of FSS plot within the upper and lower bounds of the FSS correlation in **Figure 2** at an effective normal stress of 50 kPa. In addition, the average of the data is in agreement with the average trend line for an effective normal stress of 50 kPa, which is the relevant value for the shallow failures observed in the levees.

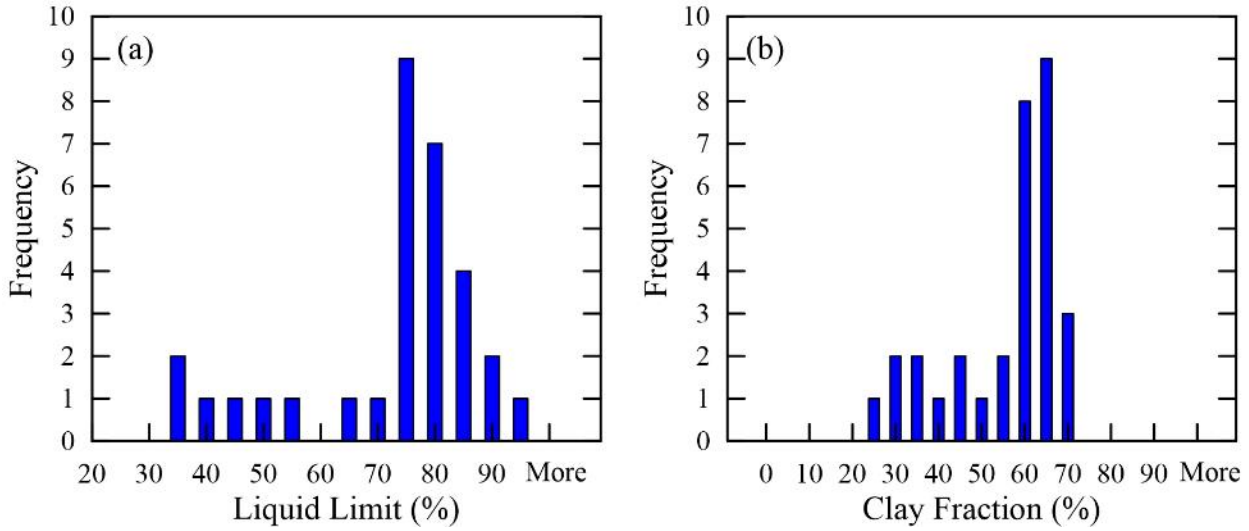

Figure 17: Histograms of (a) LL and (b) CF for slope instability areas along the Dallas Floodway.

CRITICAL FAILURE SURFACE AND APPLICABLE FACTORS OF SAFETY

For fine-grained soil embankments and cutslopes, the critical semi-circular to planar failure surface should be located using the drained peak strength of the compacted and/or natural soil because this is the location of the most detrimental shear stresses in the slope. This is important because the compacted embankment or natural slope starts at a peak strength, which can be reduced to a fully softened condition with time and the appropriate shear and environmental conditions. However, a fully softened condition may not occur over the entire length of the failure surface at the time of failure due to applied shear stresses and variations in the weathering and softening processes. As a result, the critical failure surface also should be located using a stress-dependent FSS envelope and the lowest FS for these two failure surfaces should be used for design. After locating these two static failure surfaces, various shear strengths should be considered with corresponding minimum values of FS.

Figure F-1 in **Appendix F** of the Supplemental Data shows that a large difference can exist between drained fully softened and residual strengths for soil with different plasticity. The difference between FSS and residual strength is significant for liquid limits greater than 50 so the potential for progressive failure is greater in these soils. **Figure F-1** also shows that the difference between FSS and residual strengths is greater for shallow failure surfaces than for deeper failure surfaces. As a result, the following two FS scenarios are presented for shallow failure surfaces in overconsolidated cut and compacted fill slopes:

1. Use the FSS that represents the level of field disaggregation and loss of structure due to cycles of wetting and drying, and assume full softening can occur over the service life of the structure and meet or exceed a two-dimensional FS of 1.5 or 1.4 for levees under U.S. Army Corps of Engineering (2003) Engineer Manual EM 1110-2-1902 – Slope Stability. If a three-dimensional stability analysis is used, higher values of FS should be satisfied especially for concave slopes (Stark and Ruffing, 2017).

2. Use the drained residual strength for materials that will undergo softening and shear displacement due to applied shear stresses and meet or exceed a two-dimensional FS of unity (1.0) if a ring shear residual strength is used. This is not a conservative recommendation because the required FS is only unity (1.0), not 1.5, and Mesri and Shahein (2003) show a portion of the failure surface in first-time slides can mobilize a residual strength condition. If a reversal DS large displacement strength is used to measure the residual strength, the FS should meet or exceed a two-dimensional FS of 1.1. The residual friction angle (ϕ'_r) in clay embankments can be estimated from the updated empirical residual strength correlation in **Figure G-1 in Appendix G.**

SUMMARY

This paper presents techniques for measuring the FSS and using FSS correlations for slope, embankment, dam, and levee design. A summary of the main points of the paper are:

1. The fully softened strength (FSS) is applicable for shallow cut slope and compacted embankment soils because it represents the strength remaining after the effects of

mechanical overconsolidation, compaction, desiccation, and/or other strengthening processes have been significantly reduced or removed due to applied shear stresses, wetting, stress relief, swelling, and/or weathering.

2. The relevant mode of shear for first-time slides in natural cut slopes and compacted embankments is closer to consolidated-drained (CD) triaxial compression than ring shear or direct shear tests.
3. Testing presented herein shows ring shear and direct shear devices yield similar FSS envelopes for the three CF groups in the Stark and Eid (1997) FSS correlation. This is expected because ring shear and direct shear devices induce failure along a nearly horizontal surface and involve similar consolidation and shearing conditions.
4. Data presented herein shows the CD triaxial compression conversion factor of 2.5^0 for ring shear and direct shear tests results is reasonable to slightly conservative for shallow failure surfaces by about 0.5^0. As a result, accurate ring shear and direct shear test results should plot below the FSS correlation in **Figure 2** because the FSS correlation reflects the CD triaxial compression mode of shear, i.e., RS increased by 2.5^0. This is also in agreement with Duncan et al. (2014), which state that triaxial compression tests produce higher friction angles than the direct shear test.
5. It is recommended that histograms be used to select representative values of LL and CF for use in the FSS empirical correlation instead of statistics because they can be skewed by some low values that probably will not control slope or retaining wall stability. Slope or embankment specific values of LL and CF should be used to estimate the FSS strength envelope and not overall site index properties.

6. The Castellanos et al. (2016) and Castellanos (2014) FSS correlations are unreliable and should not be used even for planning level decisions (see **Figure 11**).
7. If a range of soils will be considered for a borrow source or project alignment, a minimum of one soil from each CF group should be shear tested for the full range of effective normal stresses to "anchor" the FSS correlation and produce reasonable stress-dependent FSS envelopes for final design.

ACKNOWLEDGEMENTS

The authors gratefully acknowledge the support of Juan Sebastian Lopez-Zhindon, Daniel O'Donnell, and Andony Landivar-Macias with the data analysis and laboratory testing that they provided while students at the University of Illinois at Urbana-Champaign. The findings and opinions in this paper are solely those of the authors.

REFERENCES

American Society for Testing and Materials (ASTM). (2011). "Standard test method for direct shear test of soils under consolidated drained conditions," (*D3080-11), 2011 annual book of ASTM standards,* Vol. 04.08, West Conshohocken, Pa.

947 American Society for Testing and Materials (ASTM). (2008a). "Standard test method for liquid
948 limit, plastic limit, and plasticity index of soils," *(D 4318) 2008 annual book of ASTM*
949 *standards*, Vol. 04.08, West Conshohocken, Pa.
950 American Society for Testing and Materials (ASTM). (2011). "Standard Test Method for
951 Consolidated Drained Triaxial Compression Test for Soils," (D7181-11), ASTM International,
952 West Conshohocken, PA, 2011
953 American Society for Testing and Materials (ASTM). (2010). "Standard test method for torsional
954 ring shear test to determine drained fully softened shear strength and nonlinear strength
955 envelope of cohesive soils (using normally consolidated specimen) for slopes with no pre-
956 existing shear surfaces," (*D7608-10), 2010 annual book of ASTM standards*, Vol. 04.08, West
957 Conshohocken, Pa.
958 American Society for Testing and Materials (ASTM). (2008b). "Standard test method for particle-
959 size distribution (Gradation) of fine-grained soils using sedimentation analysis," (*D 7928)*
960 *2008 annual book of ASTM standards*, Vol. 04.08, West Conshohocken, Pa.
961 Bishop, A.W., D.L. Webb, and P.I. Lewin (1965). "Undisturbed samples of London clay from the
962 Ashford Common shaft: strength-effective stress relationship," Géotechnique, 15(1), 1-31
963 Castellanos, B. A. (2014). "Use and Measurement of Fully Softened Shear Strength," Ph.D.
964 dissertation, Virginia Tech, Blacksburg, VA, p. 805,
965 https://www.dropbox.com/s/0k0ym51d8jdmn4v/Castellanos-FSS-Thesis-2014.pdf?dl=0.
966 Castellanos, B. A., Brandaon, T.L., Stephens I., and Walshire, L. (2013) "Measurement of fully
967 sofetend shear strength," Geo-Congress-2013. ASCE, San Diego, California, USA, 234-244.
968 doi: http://dx.doi.org/10.1061/9780784412787.024.

969 Castellanos, B. A., Brandon, T. L., and VandenBerge, D. R. (2016). "Correlations for Fully
970 Softened Shear Strength Parameters," *Geotechnical Testing Journal*, 39(4), 2016, 568-581,
971 https://doi.org/10.1520/GTJ20150184, ISSN 0149-6115.
972 Chandler, R.J. and Skempton, A.W. (1974). "The design of permanent cutting slopes in stiff
973 fissured clays," *Geotechnique*, London, England, 24(4), 457-466.
974 Cooper, M. R., Bromhead, E. N., Petley, D. J., an& Grant, D. I. (1998). "The Selborne cutting
975 stability experiment," *Geotechnique*, London, England, 48(1), 83–101, doi:
976 10.1680/geot.1998.48.1.83.
977 Crabb, G. I. and Atkinson, J. H. (1991). "Determination of soil strength parameters for the analysis
978 of highway slope failures," In Slope stability engineering: developments and applications (ed.
979 R. J. Chandler), London: Thomas Telford, pp. 13–18.
980 Duncan, J. M., Wright, S.G., and Brandon, T. L. (2014). *Soil Strength and Slope Stability*, John
981 Wiley and Sons, Hoboken, N.J., 317 p.
982 Eid, H. T. (1996). "Drained Shear Strength of Stiff Clays for Slope Stability Analyses," Ph.D.
983 thesis, University of Illinois, Urbana-Champaign, IL, p. 242.
984 Eid, H.T. and Rabie, K.H. (2017). "Fully Softened Shear Strength for Soil Slope Stability
985 Analyses," *International Journal of Geomechanics*, ASCE, 17(1), pp. 04016023-1 -
986 04016023-10, http://dx.doi.org/10.1061/(ASCE)GM.1943-5622.0000651.
987 Eid, H.T. and Rabie, K.H. (2018). Closure to: "Fully Softened Shear Strength for Soil Slope
988 Stability Analyses," *International Journal of Geomechanics*, ASCE, 18(4), pp. 07018002-1 -
989 07018002-3.

990 Gamez, J. and Stark, T.D., (2014). “Fully Softened Shear Strength at Low Stresses for Levee and
991 Embankment Design,” *J. Geotech. Geoenviron. Engrg.*, ASCE, 140(9), pp. 06014010-1-
992 06014010-6.
993 Gibson, R.E., (1953) "Experimental Determination of the True Cohesion and True Angle of
994 Internal Friction in Clays," Proceedings of the Third International Conference on Soil
995 Mechanics and Foundation Engineering, Zurich, Volume 1, August 1953, pp. 126-130.
996 Kayyal, M.K. and Wright, S.G. (1991). “Investigation of Long-Term Strength Properties of Paris
997 and Beaumont Clays in Earth Embankments,” Research Project No. CTR 3-8-89/1-1195-2F,
998 Center for Transportation Research, University of Texas, Austin, TX, Research Report 1195-
999 2F, 123 pp.
1000 Lade, P. V. (2010). “The mechanics of surficial failure in soil slopes,” *J. Eng. Geo.*, ASCE, 114(1-
1001 2), 57–64.
1002 Lupini, J. F., Skinner, A. E., and Vaughan, P. R. (1981). "The drained residual strength of cohesive
1003 soils," *Geotechnique*, London, England, 31(2), 18 1-213.
1004 Mesri, G., and Shahien, M. (2003). “Residual shear strength mobilized in first-time slope failures,”
1005 J. Geotech. Geoenviron. Eng., 129(1), 12–31
1006 Mesri, G. and Cepeda-Diaz, A. F. (1986). “Residual Shear Strength of Clays and Shales,”
1007 *Geotechnique*, *36*(2), 269-274.
1008 Osano S. N. (2012) “Direct shear box and ring shear test comparison: Why internal angle of friction
1009 vary,” Journal of Engineering Indian Centre for Advanced Scientific and Technological
1010 Research (Icastor),” 5(2), pp. 77 – 93.
1011 Schofield, A.N. and Wroth, C.P. (1968). *Critical State Soil Mechanics*, McGraw-Hill, London,
1012 228 p.

Skempton, A.W. (1954). “The Pore-Pressure Coefficients A and B,” Géotechnique, 4(4), 143–147.

Skempton, A.W. (1970). “First-Time slides in over-consolidated clays,” *Geotechnique*, London, England, 20(3), 320–324.

Skempton, A. (1977). “Slope stability of cutting in brown London clay,” *Proc. 9th Int. Conf. on Soil Mech. and Found. Engrg.*, Society of Soil Mech. And Found. Engrg., Tokyo, 261–270.

Stark, T.D. (1987). “Mechanisms of Strength Loss in in Stiff Clays,” Ph.D. dissertation, Virginia Tech, Blacksburg, VA, p. 286.

Stark, **T.D. (2017).** Discussion of "Correlations for Fully Softened Shear Strength Parameters," by Castellanos, B.A., Brandon, T.L., and VandenBerge, D.R., *Geotechnical Testing Journal*, ASTM Intl., 40(3), May, 2017, pp. 517-525, **DOI:** 10.1520/GTJ20160148.

Stark, T. D., Choi, H., and McCone, S. (2005). “Drained shear strength parameters for analysis of landslides,” *J. Geotech. Geoenviron. Engrg.*, ASCE, **131**(5): 575–588.

Stark, T.D. and Duncan, J.M. (1991). "Mechanisms of Strength Loss in Stiff Clays," *J. Geotech. Geoenviron. Engrg.*, **117**(1): 139-154.

Stark, T. D. and Eid, H.T. (1993). "Modified Bromhead Ring Shear Apparatus," *Geotechnical Testing Journal*, ASTM, 16(1), March, 100-107.

Stark, T. D. and Eid, H.T. (1997). “Slope stability analyses in stiff fissured clays,” *J. Geotech Geoenviron. Engrg.*, **123** (4): 335–343.

Stark, T. D. and Hussain, M. (2013). “Drained shear strength correlations for slope stability analyses,” *J. Geotech. Geoenviron. Engrg.*, **139** (6): 853–862.

Stark, T.D. and Ruffing, D.G. (2017). "Selecting Minimum Factors of Safety for 3D Slope Stability Analyses," *Proceedings of Specialty Conf. GEO-Risk-2017*, ASCE, Denver, CO, June 4-7, 2017, Geotechnical Special Publication 283, pp. 259-266.

1037 Stark, T.D., Jafari, N.H., Lopez-Zhindon, S., and Baghdady, A. (2017). "Unsaturated and transient
1038 seepage analysis of San Luis Dam," *J. Geotechnical and Geoenvironmental Eng., 143(2),*
1039 February, 2017, pp. 04016093-1 - 04016093-15, DOI: 10.1061/(ASCE)GT.1943-
1040 5606.0001602.
1041 Stephens, I., Olsen, R., Manning, A., Galan-Comas, G., Ahue, W., Pearson, M., Lee, L., and
1042 Coffing, L. (2011). "Trinity River, Dallas, TX, Floodway System: Fully-softened Shear
1043 Strength Testing Program," US Army Corps of Engineers, Ft. Worth, TX.
1044 Take, W.A. and Bolton, M.D. (2011). "Seasonal ratcheting and softening in clay slopes, leading
1045 to first-time failure," *Géotechnique*, London, England, 61(9), 757-769).
1046 Terzaghi, K. (1936). "Stability of slopes of natural clay," *Proceedings of the 1st International*
1047 *Conf. on Soil Mechanics and Foundation Engineering*, 1, 161–165.
1048 Terzaghi, K., Peck, R., and Mesri, G. (1996). *Soil Mechanics in Engineering Practice.* John Wiley
1049 and Sons, Inc., New York.
1050 U.S. Army Corps of Engineers (USACE) (1970). "Engineer Manual: Stability of Earth and Rock-
1051 Fill Dams," EM 1110-2-1902, Waterways Experiment Station, Vicksburg, MS.
1052 Wright, S. G. (2005). *Evaluation of soil shear strengths for slope and retaining wall stability*
1053 *analyses with emphasis on high plasticity clays*. Center for Transportation Research,
1054 University of Texas at Austin, 100 p.
1055 Wright, S. G., Zornberg, J. G., and Aguettant, J. E. (2007). "The fully softened shear strength of
1056 high plasticity clays," Center for Transportation Research. University of Texas at Austin,
1057 Report No. FHWA/TX-07/0-5202-3 200, 132 p.
1058

FULLY SOFTENED SHEAR STRENGTH MEASUREMENT AND EMPIRICAL CORRELATION

Timothy D. Stark[3] and Rodrigo Fernandez[4]

List of Figures:

Fig. 1: Mobilized drained shear strength in first-time slope failures in brown London Clay and comparison with the results of drained laboratory shear tests.

Fig. 2: Updated drained fully softened secant friction angle correlation for: (a) CF ≤ 20% and (b) CF > 20%.

Fig. 3: Comparison of fully softened secant angles obtained from CD triaxial compression and RS tests.

Fig. 4: FSS strength envelopes for Panoche Shale from CD triaxial, ring shear, and direct shear FSS tests.

Fig. 5: Shear stress ratio versus shear displacement for direct shear and ring shear tests on Panoche Shale from Eid (1996).

Fig. 6: FSS strength envelopes from RS and DS testing on Duck Creek Shale and FSS empirical correlation for CF group ≤ 20%.

Fig. 7: FSS strength envelopes from RS and DS testing on Pierre Shale and FSS empirical correlation for CF group 25% ≤ CF ≤ 45%.

[3] Professor, Dept. of Civil and Environmental Engineering, Univ. of Illinois, 205 N. Mathews Ave., Urbana, IL 61801-2352. E-mail: tstark@illinois.edu

[4] Graduate Research Assistant, Dept. of Civil and Environmental Engineering, Univ. of Illinois, 205 N. Mathews Ave., Urbana, IL 61801-2352. E-mail: rodrigo.fernandez0312@gmail.com

Fig. 8: FSS strength envelopes from RS and DS testing on brown London Clay and FSS empirical correlation for CF group $\geq$ 50%.

Fig. 9: FSS strength envelopes from five (5) empirical correlations for Duck Creek Shale and San Francisco Bay Mud for CF $\leq$ 25%.

Fig. 10: FSS strength envelopes from five (5) empirical correlations for Oso Lacustrine Clay and Bearpaw Shale for CF 25% $\leq$ CF $\leq$ 45%.

Fig. 11: FSS strength envelopes from six (6) empirical correlations for Big Bear Claystone and Pierre Shale for CF $\geq$ 50%.

Fig. 12: Recommended power function coefficients "a" and "b" to estimate drained FSS envelopes for the three CF groups as a function of LL.

Fig. 13: Recommended power function coefficient "a" and "b" to estimate drained residual shear strength envelopes for the three CF groups as a function of LL.

Fig. 14: Measured and estimated drained FSS and residual strength envelopes for upstream and downstream slopewash at San Luis Dam.

Fig. 15: Histograms of: (a) LL and (b) CF for heavily over-consolidated clay project site.

Fig. 16: Histograms of: (a) LL and (b) CF for a particular slope in the heavily over-consolidated clay in the project site shown in **Figure 15**.

Fig. 17: Histograms of (a) LL and (b) CF for slope instability areas along the Dallas Floodway.

List of Tables:

Table 1: Comparison of brown London Clay shear strength parameters.

Table 2: Difference in secant FSS friction angles from RS and CD triaxial compression (from Eid, 1996).

Table 3: Secant FSS friction angles from RS, DS, and CD triaxial compression tests on Panoche Shale from Eid (1996).

Table 4. Summary of factor of safety for upstream slope of San Luis Dam.

Table 5: Summary of LL and CF for a project site involving a mechanically overconsolidated clay.

SUPPLEMENTAL DATA

Appendix A

Summary Soils used for Fully Softened Strength Ring Shear Testing

Table A-1: Summary of soils used for fully softened strength (FSS) ring shear testing with the soils tested during this study indicated by "^:.

Soil Number	Soil Name	Site Location	LL (%)	PL (%)	CF (%)	Activity (PI/CF)
1	*Glacial till	Urbana, IL	24	16	18	0.44
^2	*^Glacial till	Urbana, IL	20	15	18	0.33
3	*Loess	Vicksburg, MS	28	18	10	1.00
^4	*^Glacial Till	Spring Valley, IL	29	22	24	0.29
^5	*^Colluvium	Charleston, WV	32	21	45	0.24
6	*Sandy lean clay	Dallas, TX	35	13	25	0.88
^7	*^Colluvium	Charleston, WV	36	23	45	0.29
8	#Duck Creek shale	Fulton, IL	37	25	19	0.63
9	*Slide debris	San Francisco, CA	37	26	28	0.39
^10	*^Western Oso River	Oso, WA	38	21	31	0.55
11	*Colluvium	Vallejo, CA	39	22	36	0.47
^12	*^Colluvium	Charleston, WV	40	21	46	0.41
13	*Upstream Slopewash material	Los Banos, CA	40	24	34	0.47
14	*Downstream Slopewash material	Los Banos, CA	42	22	35	0.57
15	*Crab Orchard shale	Peoria, IL	44	24	32	0.63
16	*Failure plane debris	Brillant, OH	44	19	39	0.64
17	#Colorado shale	Montana, MT	46	25	73	0.29
18	*Panoche mudstone	San Francisco, CA	47	27	41	0.49
19	*Sandy lean clay	Dallas, TX	49	19	17	1.76
^20	*^Eastern Oso River	Oso, WA	52	25	51	0.53
21	*Panoche shale	San Francisco, CA	53	29	50	0.48
22	*Colluvium	Marietta, OH	54	25	48	0.6
23	*Slide plane material	Los Angeles, CA	55	24	27	1.15
24	*Silty clay	Esperanza Dam, Ecuador	55	40	29	0.52
25	*Illinois Valley shale	Peru, IL	56	24	45	0.71
26	*Bel Air (GMX-1 @ 17 ft. depth)	Los Angeles, CA	60	33	45	0.6
27	#Comanche shale	Proctor Dam, TX	62	32	68	0.44
28	*Breccia material	Manta, Ecuador	64	41	25	0.92
29	*Silty clay	La Esperanza Dam, Ecuador	64	41	21	1.1

30	*High plasticity clay	Dallas, TX	65	17	43	1.12
^31	*^High plasticity clay (NoVA)	Northern Virginia	65	39	24	0.96
32	*Shale	Dallas, TX	73	32	60	0.68
33	*Claystone	Big Bear, CA	75	22	54	0.98
34	*Siltstone/Claystone	Orange County, CA	75	37	48	0.79
35	*Bay mud	San Francisco, CA	76	41	16	2.19
36	#Patapsco shale	Washington, D.C.	77	25	59	0.88
^37	*^Buckshot clay	Vicksburg, MS	66	28	40	0.95
^38	*^Buckshot clay - VT	Vicksburg, MS	78	26	69	0.75
39	*Pierre shale	Rapid City, SD	80	49	56	0.88
40	#Pierre shale	Limon, CO	82	30	42	1.24
41	*Shear surface (depth 19.8 m)	Los Angeles, CA	82	31	50	1.02
42	*Shear surface	Los Angeles, CA	83	29	52	1.04
43	*Madisette Clay	Madisette, CA	83	29	52	1.04
44	*^Eagle Ford Shale	Dallas, TX	85	27	70	0.82
45	*Lower Pepper shale	Waco Dam, TX	94	26	77	0.88
46	*Serpentinite clay	Marion County, CA	95	27	54	1.26
^47	*^Sentinel Butter Formation S#4	Watford, ND	96	23	55	1.32
48	#Brown London clay	Bradwell, England	101	35	66	1
49	#Cucaracha shale	Panama Canal	111	42	63	1.1
50	#Denver shale	Denver, CO	121	37	67	1.25
51	#Bearpaw shale	Saskatchewan, Canada	128	27	43	2.35
^52	*^Sentinel Butter Formation S#1	Watford, ND	135	26	67	1.63
53	*Pierre shale	Newcastle, WY	137	30	54	1.98
54	*Oahe firm shale	Oahe Dam, SD	138	41	78	1.24
^55	*^Sentinel Butter Formation S#2	Watford, ND	139	25	70	1.63
56	#Taylor shale	San Antonio, TX	170	39	72	1.82
57	#Pierre shale	Reliance, SD	184	55	84	1.54
58	*Oahe bentonitic shale	Oahe Dam, SD	192	47	65	2.23
59	*Lea Park bentonitic shale	Saskatchewan, Canada	253	48	65	3.15
60	#Bearpaw shale	Ft. Peck Dam, MT	288	44	88	2.77

NOTES:

* Samples not ball-milled

Index properties from Mesri and Cepeda-Diaz (1986) and sample ball-milled
^ Samples tested during this study

Appendix B

Shear Stress-Shear Displacement Relationships from Direct Shear and Ring Shear Testing

To further investigate the values of FSS measured using RS and DS devices, DS tests were conducted herein on soils that had already been tested in RS. In particular, at least two soils from each of the three CF fractions groups in the Stark and Eid (1997) FSS correlation (see **Figure 2**) were tested to augment the comparison of RS and DS values of FSS started by Eid (1996). The measured shear stress-shear displacement relationships for the RS and DS tests on the soils for each CF group are presented in **Appendix B**. The plots of the FSS strength envelopes obtained from the RS and DS devices for the CF groups: CF ≤ 20% (Duck Creek Shale), 25 ≤ CF ≤ 45% (Pierre Shale), and CF ≥ 50% (Brown London Clay) are presented in **Figure 6, Figure 7,** and **Figure 8**, respectively. The strength envelopes for the other three comparisons for CF groups: 20% ≤ CF (Urbana Till), 25 ≤ CF ≤ 45% (NoVA Clay), and CF ≥ 50% (Eagle Ford Shale) are shown in **Appendix C**. As expected, the DS and RS devices yield similar FSS strength envelopes regardless of the CF. This reaffirms the data and conclusion generated by Eid (1996).

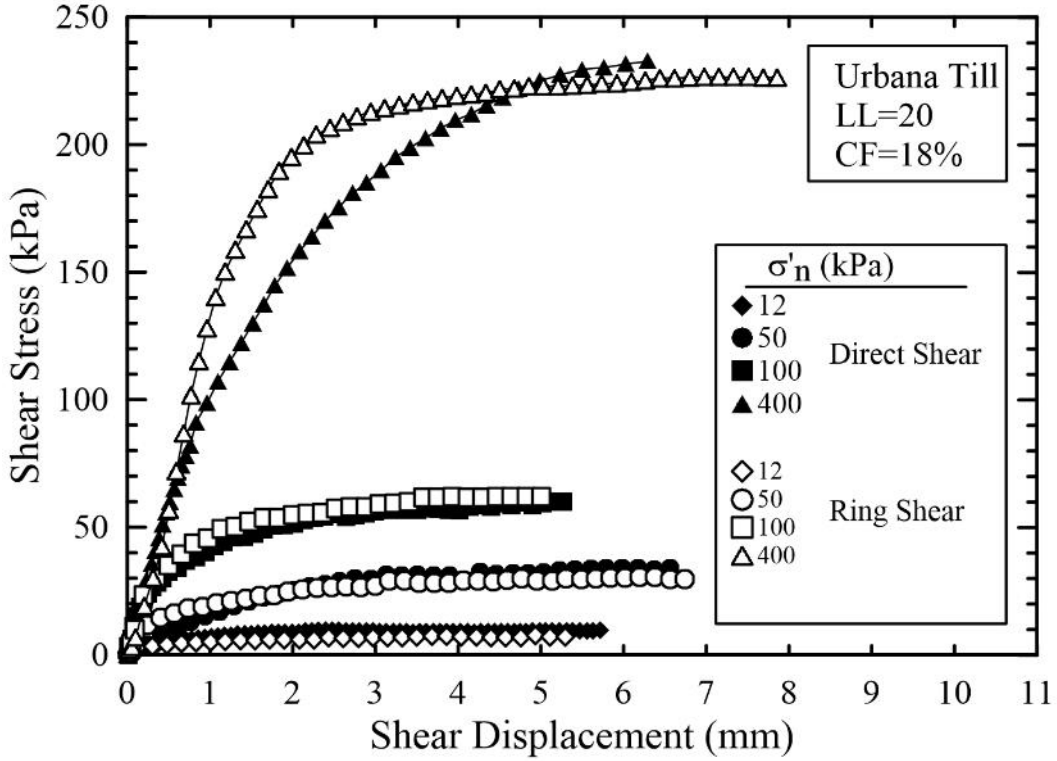

Figure B-1: Shear stress-shear displacement relationships from direct shear and ring shear testing on Urbana Till for CF group CF ≤ 20%.

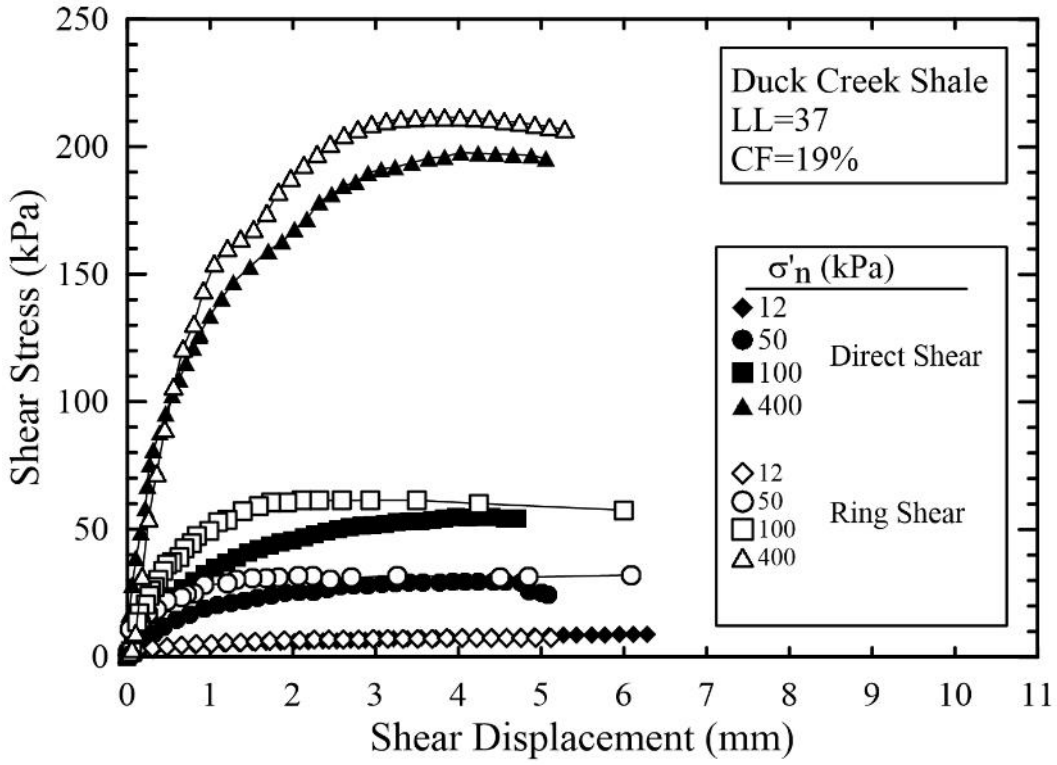

Figure B-2: Shear stress-shear displacement relationships from direct shear and ring shear testing on Duck Creek Shale for CF group CF ≤ 20%

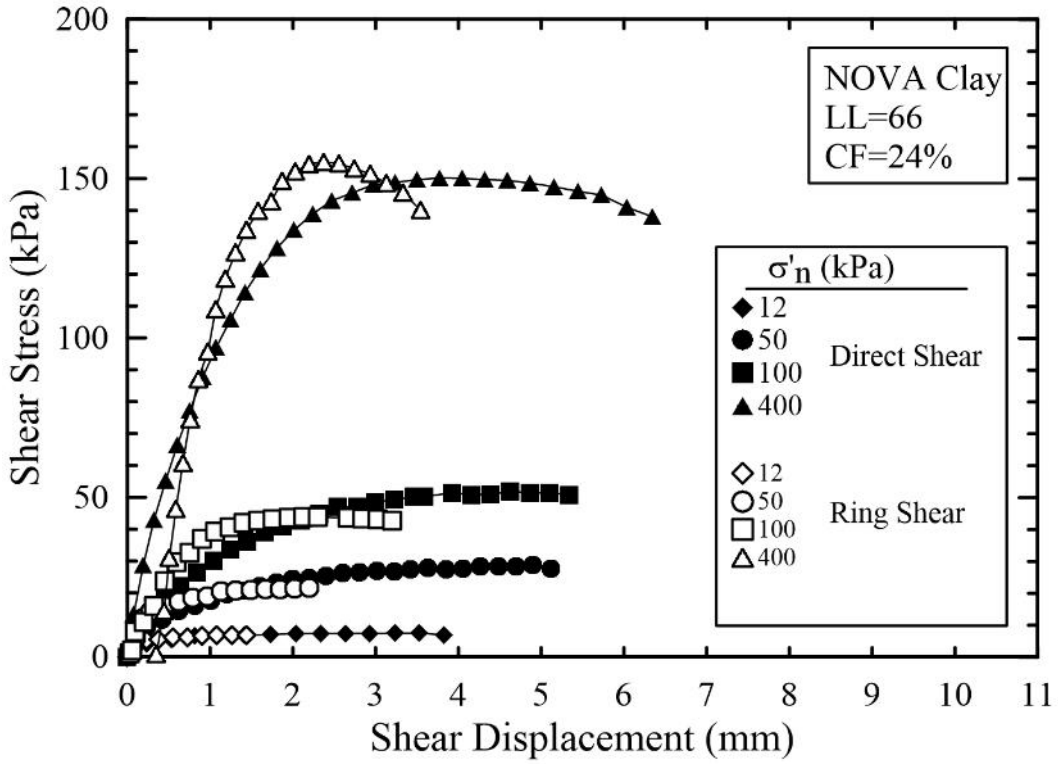

Figure B-3: Shear stress-shear displacement relationships from direct shear and ring shear testing on Northern Virginia Clay for CF group $25 \leq CF \leq 45\%$.

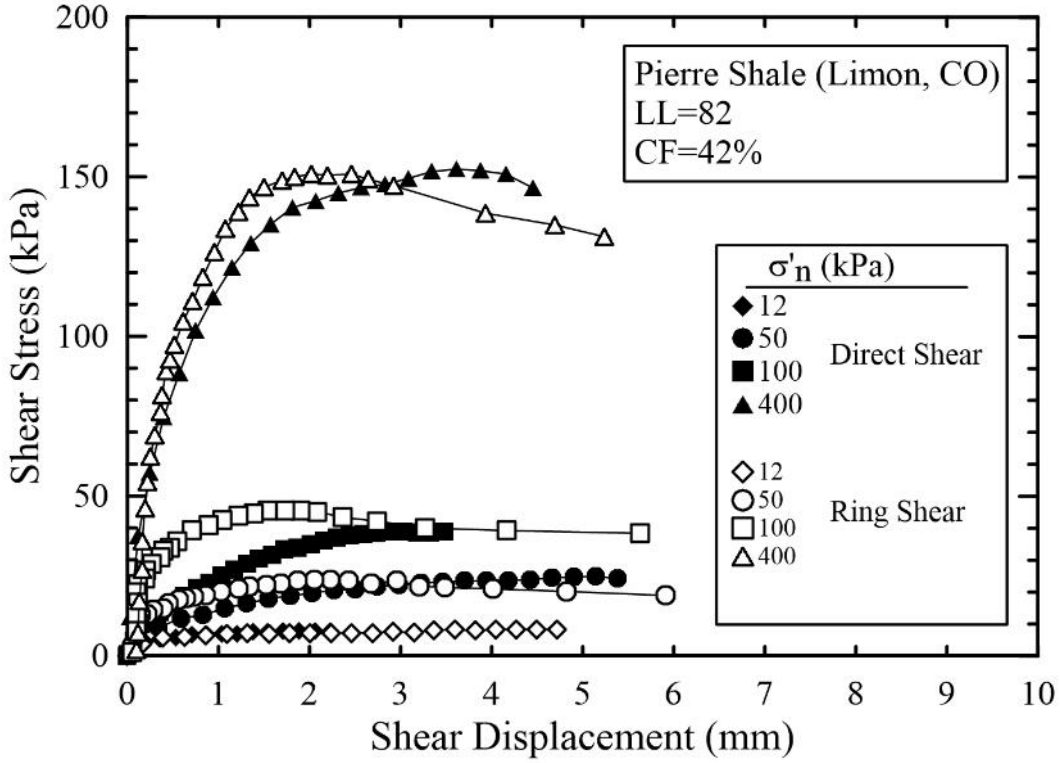

Figure B-4: Shear stress-shear displacement relationships from direct shear and ring shear testing on Pierre Shale for CF group 25% ≤ CF ≤ 45%.

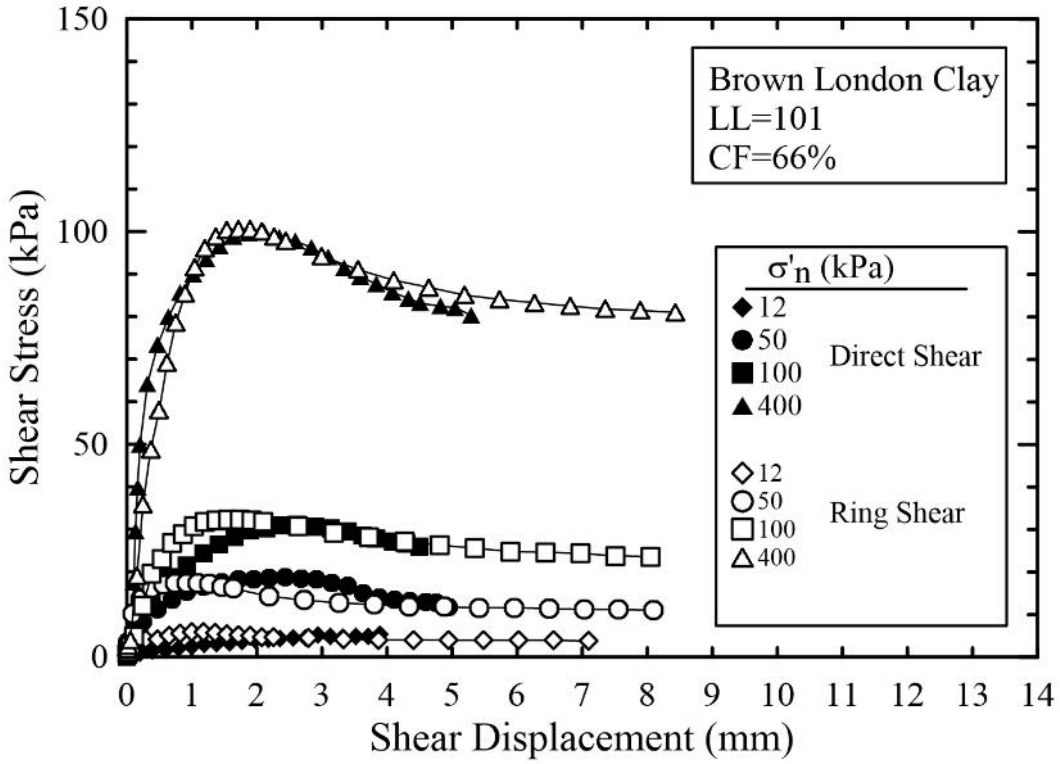

Figure B-5: Shear stress-shear displacement relationships from direct shear and ring shear testing on Brown London Clay for CF group CF≥50%.

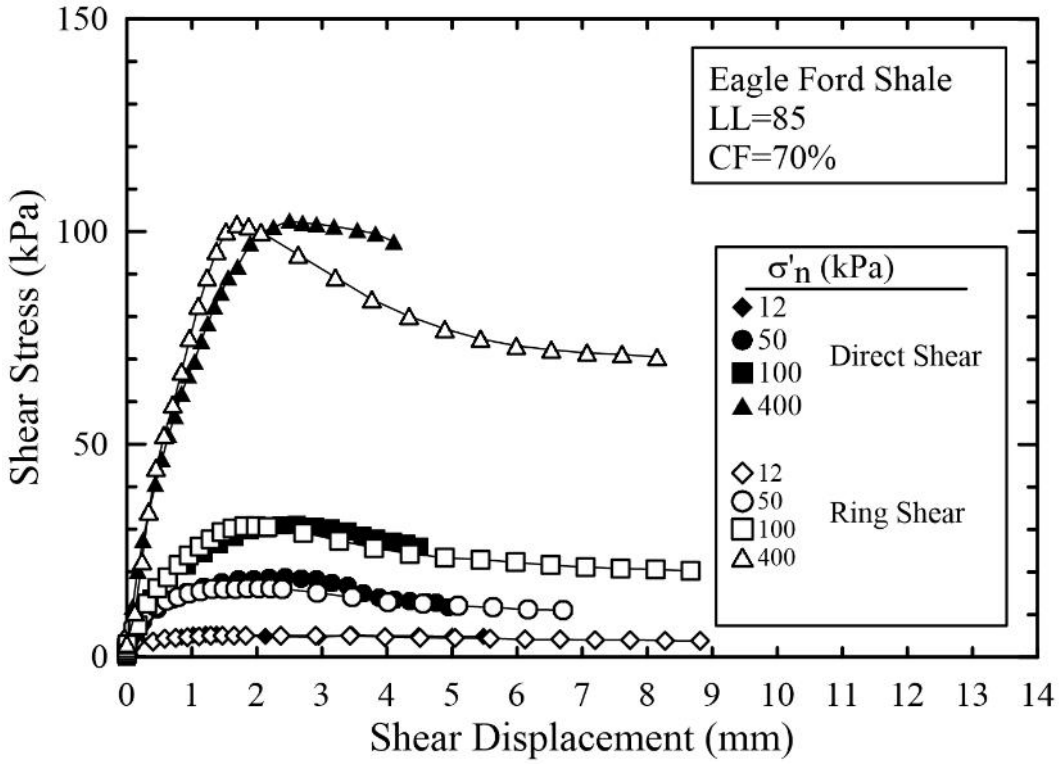

Figure B-6: Shear stress-shear displacement relationships from direct shear and ring shear testing of Eagle Ford Shale for CF group CF≥50%.

Appendix C

Strength Envelopes from Direct Shear and Ring Shear Testing

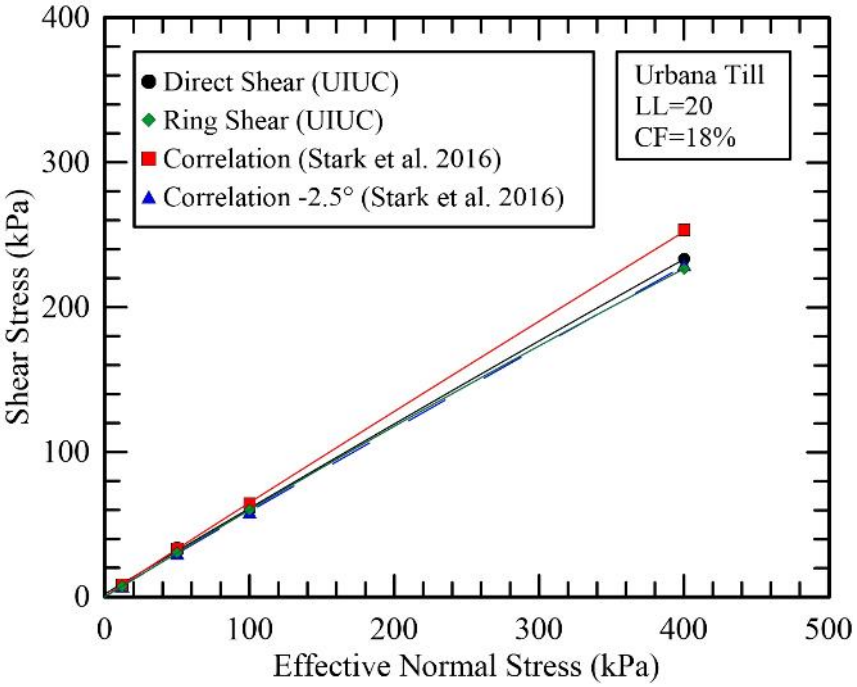

Figure C-1: FSS strength envelopes from direct shear and ring shear testing on Urbana Till and FSS empirical correlation by Stark and Eid (1997) for CF group CF ≤ 20%.

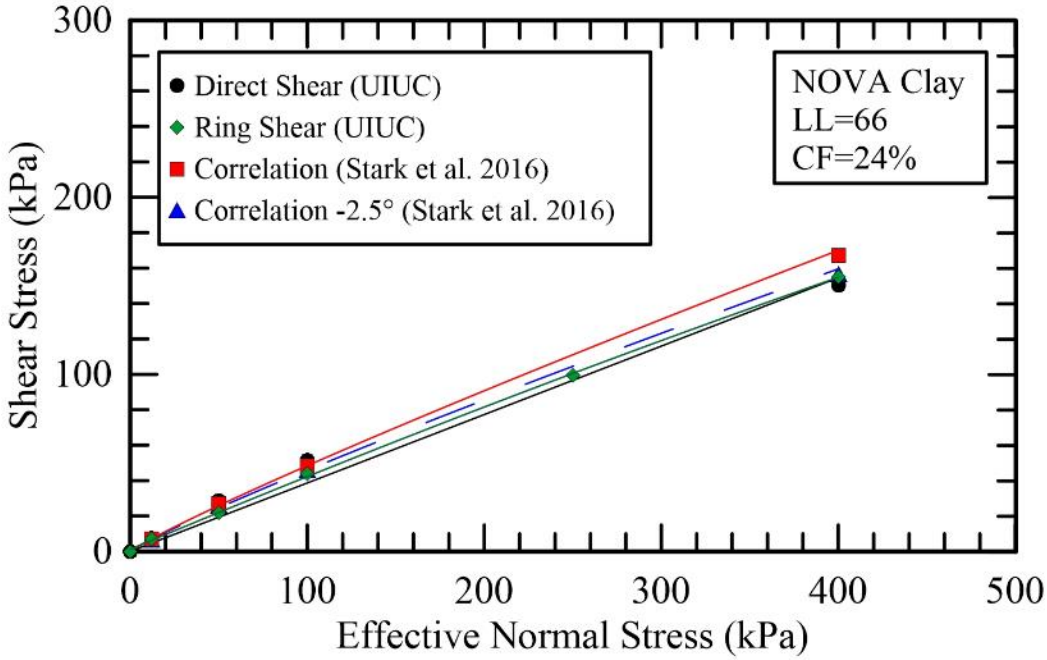

Figure C-2: FSS strength envelopes from direct shear and ring shear testing on Northern Virginia (NoVA) Clay and FSS empirical correlation by Stark and Eid (1997) for CF group 25% ≤ CF ≤ 45%.

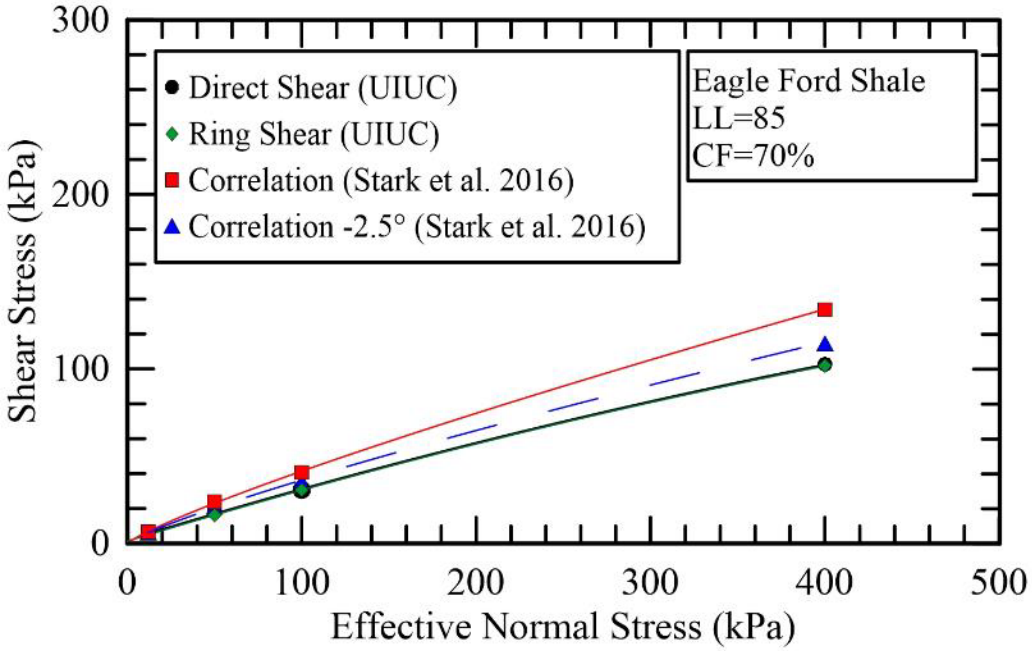

Figure C-3: FSS strength envelopes from direct shear and ring shear testing on Eagle Ford Shale and FSS empirical correlation by Stark and Eid (1997) for CF group CF≥50%.

Appendix D

Equations for trend lines in FSS Empirical Correlation

The current study refined the equations used to represent the trend lines in the FSS empirical correlation by Stark and Eid (1997) and its updates. The values of LL and CF used in the equations should be in terms of whole numbers not decimal form. These equations are used in the EXCEL spreadsheet mentioned above that can be used to estimate the FSS and residual strength envelopes for a range of input parameters and assess the sensitivity of the strength envelope to the various CF groups. The spreadsheet is available at **www.tstark.net** and can be used and distributed to the geotechnical profession.

A second degree polynomial adequately represents the FSS trend lines for all CF groups and all four effective normal stresses in Gamez and Stark (2014). The set of equations developed for CF Group No. 1 ($20\% \leq CF$) trend lines, which has measured values of LL ranging from 30% to less than 80% ($30\% \leq LL \leq 80\%$) are:

$$\left(\phi'_{FSS}\right)_{\sigma'_n=12kPa} = 35.33 - 5.85x10^{-2}(LL) + 9.71x10^{-5}(LL)^2 \quad (D.1)$$

$$\left(\phi'_{FSS}\right)_{\sigma'_n=50kPa} = 34.85 - 0.07929(LL) + 2.35x10^{-4}(LL)^2 \quad (D.2)$$

$$\left(\phi'_{FSS}\right)_{\sigma'_n=100kPa} = 34.39 - 0.0863(LL) + 2.66x10^{-4}(LL)^2 \quad (D.3)$$

$$\left(\phi'_{FSS}\right)_{\sigma'_n=400kPa} = 34.76 - 0.13(LL) + 4.71x10^{-4}(LL)^2 \quad (D.4)$$

NOTE: The values of LL used in the equations should be in terms of whole numbers not decimal form.

Another set of equations was developed for the trend lines in CF Group No. 2 ($25\% \leq CF \leq 45\%$) with measured LL values ranging from 30% to less than 130% ($30\% \leq LL \leq 130\%$):

$$\left(\phi'_{FSS}\right)_{\sigma'_n=12kPa} = 38.10 - 1.19x10^{-1}(LL) + 2.48x10^{-4}(LL)^2 \quad (D.5)$$

$$\left(\phi'_{FSS}\right)_{\sigma'_n=50kPa} = 36.18 - 0.1143(LL) + 2.354x10^{-4}(LL)^2 \quad (D.6)$$

$$\left(\phi'_{FSS}\right)_{\sigma'_n=100kPa} = 33.11 - 0.107(LL) + 2.2x10^{-4}(LL)^2 \quad (D.7)$$

$$\left(\phi'_{FSS}\right)_{\sigma'_n=400kPa} = 30.7 - 0.1263(LL) + 3.442x10^{-4}(LL)^2 \quad (D.8)$$

NOTE: The values of LL used in the equations should be in terms of whole numbers not decimal form.

A third set of cubic equations was developed for CF Group No. 3 ($CF \geq 50\%$) with measured LL values ranging from 30% to less than 300% ($30\% \leq LL < 300\%$) as shown below:

$$\left(\phi'_{FSS}\right)_{\sigma'_n=12kPa} = 36.45 - 9.18x10^{-2}(LL) + 1.09x10^{-4}(LL)^2 - 1.10x10^{-7}(LL)^3 \quad (D.9)$$

$$\left(\phi'_{FSS}\right)_{\sigma'_n=50kPa} = 33.37 - 0.11(LL) + 2.344x10^{-4}(LL)^2 - 2.96x10^{-7}(LL)^3 \quad (D.10)$$

$$\left(\phi'_{FSS}\right)_{\sigma'_n=100kPa} = 31.17 - 0.142(LL) + 4.678x10^{-4}(LL)^2 - 6.762x10^{-7}(LL)^3 \quad (D.11)$$

$$\left(\phi'_{FSS}\right)_{\sigma'_n=400kPa} = 28.0 - 0.1533(LL) + 5.64x10^{-4}(LL)^2 - 8.414x10^{-7}(LL)^3 \quad (D.12)$$

NOTE: The values of LL used in the equations should be in terms of whole numbers not decimal form.

These equations are not valid outside of the range of measured LL values. As a result, the spreadsheet mentioned above does not present a FSS strength envelope for values of LL outside the measured ranges.

Appendix E

Equations for trend lines in Residual Strength Empirical Correlation

The mathematical expressions developed by Stark and Hussain (2013) for the residual strength correlation did not change but a presented below for completeness. The values of LL and CF used in the equations should be in terms of whole numbers not decimal form. The empirical correlation for $\square'_r$ of CF Group #1 and for LL values ranging from 30% to less than 80% (30% $\leq$ LL < 80%) are shown as Equations (E.1) to (E.4) below. The upper bound for LL is specified because no ring shear data are available outside of this LL range.

$$\left(\phi'_r\right)_{\sigma'_n=50\text{kPa}} = 39.71 - 0.29(\text{LL}) + 6.63\text{x}10^{-4}(\text{LL})^2 \quad \text{(E.1)}$$

$$\left(\phi'_r\right)_{\sigma'_n=100\text{kPa}} = 39.41 - 0.298(\text{LL}) + 6.81\text{x}10^{-4}(\text{LL})^2 \quad \text{(E.2)}$$

$$\left(\phi'_r\right)_{\sigma'_n=400\text{kPa}} = 40.24 - 0.375(\text{LL}) + 1.36\text{x}10^{-3}(\text{LL})^2 \quad \text{(E.3)}$$

$$\left(\phi'_r\right)_{\sigma'_n=700\text{kPa}} = 40.34 - 0.412(\text{LL}) + 1.683\text{x}10^{-3}(\text{LL})^2 \quad \text{(E.4)}$$

NOTE: The values of LL used in the equations should be in terms of whole numbers not decimal form.

Another set of equations was developed by Stark and Hussain (2013) for the trend lines in CF Group #2 (25%$\leq$CF$\leq$45%) and LL values ranging from 30% to less than 130% (30% $\leq$ LL < 130%) and are given below in Equations (E.5) to (E.8).

$$\left(\phi'_r\right)_{\sigma'_n=50\text{kPa}} = 31.4 - 6.79\text{x}10^{-3}(\text{LL}) - 3.616\text{x}10^{-3}(\text{LL})^2 + 1.864\text{x}10^{-5}(\text{LL})^3 \quad \text{(E.5)}$$

$$\left(\phi'_r\right)_{\sigma'_n=100\text{kPa}} = 29.8 - 3.627\text{x}10^{-4}(\text{LL}) - 3.584\text{x}10^{-3}(\text{LL})^2 + 1.854\text{x}10^{-5}(\text{LL})^3 \quad \text{(E.6)}$$

$$\left(\phi'_r\right)_{\sigma'_n=400\text{kPa}} = 28.4 - 5.622\text{x}10^{-2}(\text{LL}) - 2.952\text{x}10^{-3}(\text{LL})^2 + 1.721\text{x}10^{-5}(\text{LL})^3 \quad \text{(E.7)}$$

$$\left(\phi'_r\right)_{\sigma'_n=700\text{kPa}} = 28.05 - 0.2083(\text{LL}) - 8.183\text{x}10^{-4}(\text{LL})^2 + 9.372\text{x}10^{-6}(\text{LL})^3 \quad \text{(E.8)}$$

NOTE: The values of LL used in the equations should be in terms of whole numbers not decimal form.

Two equations are required to capture the complicated shape of the Group #3 trend lines. Stark and Hussain (2013) use a third degree polynomial represent the trend lines for CF Group #3 and for all four effective normal stresses and for 30% $\leq$ LL < 120% and the trend lines for CF Group #3 and 120% $\leq$ LL $\leq$ 300% can be represented using a linear relationship (straight line). The resulting equations are:

$$\left(\phi'_r\right)_{\sigma'_n=50kPa} = 33.5 - 0.31(LL) + 3.9x10^{-4}(LL)^2 + 4.4x10^{-6}(LL)^3 \quad (E.9)$$

$$\left(\phi'_r\right)_{\sigma'_n=100kPa} = 30.7 - 0.2504(LL) - 4.2053x10^{-4}(LL)^2 + 8.0479x10^{-6}(LL)^3 \quad (E.10)$$

$$\left(\phi'_r\right)_{\sigma'_n=400kPa} = 29.42 - 0.2621(LL) - 4.011x10^{-4}(LL)^2 + 8.718x10^{-6}(LL)^3 \quad (E.11)$$

$$\left(\phi'_r\right)_{\sigma'_n=700kPa} = 27.7 - 0.3233(LL) + 2.896x10^{-4}(LL)^2 + 7.1131x10^{-6}(LL)^3 \quad (E.12)$$

$$\left(\phi'_r\right)_{\sigma'_n=50kPa} = 12.03 - 0.0215(LL) \quad (E.13)$$

$$\left(\phi'_r\right)_{\sigma'_n=100kPa} = 10.64 - 0.0183(LL) \quad (E.14)$$

$$\left(\phi'_r\right)_{\sigma'_n=400kPa} = 8.32 - 0.0114(LL) \quad (E.15)$$

$$\left(\phi'_r\right)_{\sigma'_n=700kPa} = 5.84 - 0.0049(LL) \quad (E.16)$$

NOTE: The values of LL used in the equations should be in terms of whole numbers not decimal form.

Appendix F

Difference between Fully Softened and Residual Strengths as a Function of Liquid Limit

Figure F-1 shows that a large difference can exist between drained fully softened and residual strengths for soil with different plasticity. The difference between FSS and residual strength is significant for liquid limits greater than 50 so the potential for progressive failure is greater. **Figure F-1** also shows that the difference between FSS and residual strengths is greater for shallow failure surfaces, , than for deeper failure surfaces.

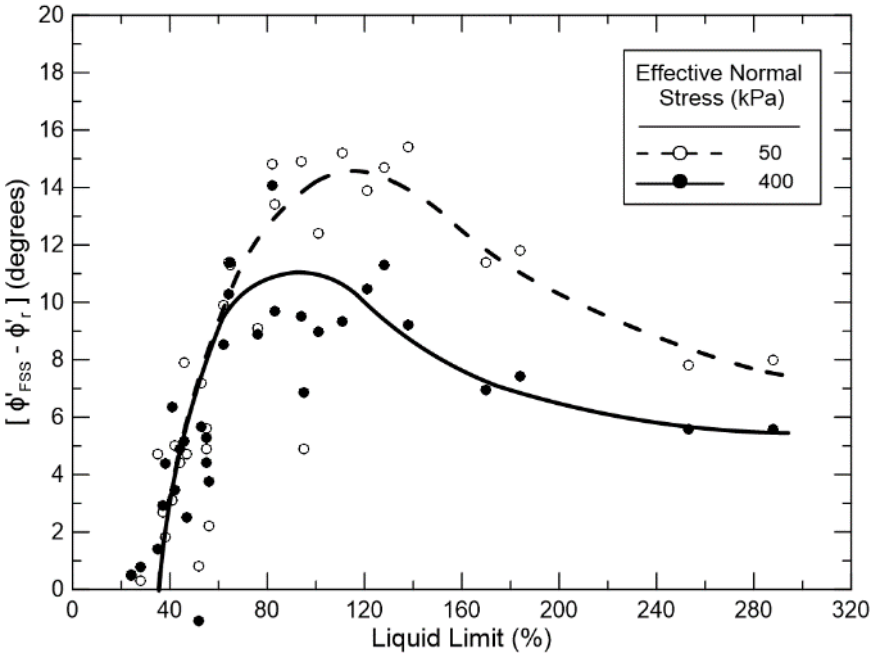

Figure F-1: Difference between secant fully softened (ϕ'_{FSS}) and residual (ϕ'_{r}) friction angles as function of liquid limit from Stark et al. (2005).

Appendix G

Residual Strength Empirical Correlation

The drained residual friction angle (ϕ'_r) of fine-grained soil in natural and compacted slopes can be estimated from the updated empirical correlation from Stark and Hussain (2013) in **Figure G-1**.

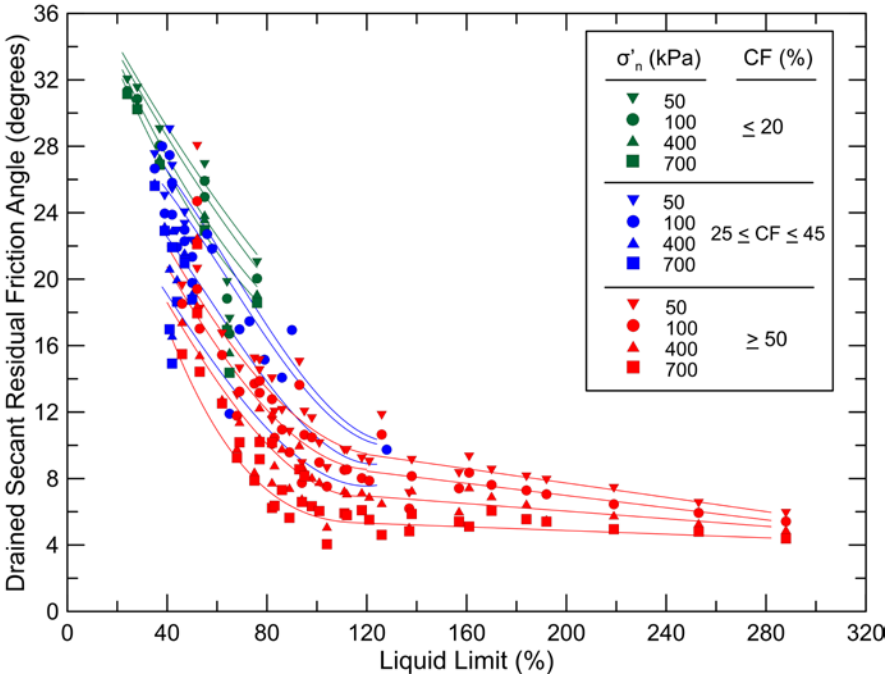

Figure G-1: Updated empirical correlation for drained residual secant friction angle based on liquid limit (LL), clay-size fraction (CF), and effective normal stress (σ'_n) after Stark and Hussain (2012).